

Predictability, Force and (Anti-)Resonance in Complex Object Control

Pauline Maurice^{1*}, Neville Hogan^{2,3}, Dagmar Sternad^{1,4,5}

1 Department of Biology, Northeastern University, Boston, MA, USA

2 Department of Mechanical Engineering, MIT, Cambridge, MA, USA

3 Department of Brain and Cognitive Sciences, MIT, Cambridge, MA, USA

4 Department of Electrical and Computer Engineering, Northeastern University, Boston, MA, USA

5 Center for the Interdisciplinary Research on Complex Systems, Northeastern University, Boston, MA, USA

***Corresponding author:** Pauline Maurice

pauline.maurice@polytechnique.org

+ 33 3 54 95 85 32

INRIA Nancy – Grand Est

615 rue du jardin botanique

54600 Villers-lès-Nancy, France

Author contributions:

D.S. conceived and designed research; P.M. performed experiments and analyzed data; P.M, D.S., and N.H. interpreted results of experiments; P.M. prepared figures; P.M. and D.S. drafted manuscript; P.M., D.S. and N.H. edited and revised manuscript; P.M., D.S. and N.H. approved final version of manuscript.

Abbreviated title: Predictability in complex object control

Abstract

24 **Abstract**
25 Manipulation of complex objects as in tool use is ubiquitous and has given humans an evolutionary
26 advantage. This study examined the strategies humans choose when manipulating an object with
27 underactuated internal dynamics, such as a cup of coffee. The object's dynamics renders the temporal
28 evolution complex, possibly even chaotic, and difficult to predict. A cart-and-pendulum model, loosely
29 mimicking coffee sloshing in a cup, was implemented in a virtual environment with a haptic interface.
30 Participants rhythmically manipulated the virtual cup containing a rolling ball; they could choose the
31 oscillation frequency, while the amplitude was prescribed. Three hypotheses were tested: 1) humans
32 decrease interaction forces between hand and object; 2) humans increase the predictability of the object
33 dynamics; 3) humans exploit the resonances of the coupled object-hand system. Analysis revealed that
34 humans chose either a high-frequency strategy with anti-phase cup-and-ball movements or a low-
35 frequency strategy with in-phase cup-and-ball movements. Counter Hypothesis 1, they did not decrease
36 interaction force; instead, they increased the predictability of the interaction dynamics, quantified by
37 mutual information, supporting Hypothesis 2. To address Hypothesis 3, frequency analysis of the
38 coupled hand-object system revealed two resonance frequencies separated by an anti-resonance
39 frequency. The low-frequency strategy exploited one resonance, while the high-frequency strategy
40 afforded more choice, consistent with the frequency response of the coupled system; both strategies
41 avoided the anti-resonance. Hence, humans did not prioritize small interaction force, but rather
42 strategies that rendered interactions predictable. These findings highlight that physical interactions with
43 complex objects pose control challenges not present in unconstrained movements.

44

45 **Key Words:** motor skill, rhythmic movements, object manipulation, prediction, interaction force,
46 impedance

47 **New and Noteworthy**

48 Daily actions involve manipulation of complex non-rigid objects which presents a challenge since
49 humans have no direct control of the whole object. We used a virtual-reality experiment and
50 simulations of a cart-and-pendulum system coupled to hand movements with impedance to analyze the
51 manipulation of this underactuated object. We showed that participants developed strategies that
52 increased the predictability of the object behavior by exploiting the object's resonance structure, but
53 did not minimize the hand-object interaction force.

54 **Introduction**

55 Using tools has been essential in human evolution, and a large variety of tools now enhance and
56 augment our daily actions. Tool-supported actions range from the simple swinging of a hammer and
57 cutting meat with a knife to more complex or exotic actions, such as eating spaghetti and cracking a
58 whip. The latter tasks are challenging and require practice because the objects themselves, spaghetti
59 and whip, are flexible hence underactuated, *i.e.* have internal degrees of freedom that are not directly
60 controlled by the user. Another seemingly mundane example is carrying a cup of coffee: the human
61 manipulates the cup that, in turn, exerts a force on the coffee that exerts forces back on the cup and the
62 hand. Complex interaction forces arise between the hand, the cup and the coffee. Despite this
63 complexity, humans are extremely skilled at interacting with such underactuated objects. Our
64 understanding of how humans achieve such dexterity is still limited and becomes an ever-growing
65 barrier to current developments in prosthesis control, brain-machine interfaces and robotic
66 rehabilitation.

67

68 Despite the abundant literature on the control of goal-directed upper-limb movements, most studies
69 have focused on free movements without physical interaction, such as reaching and pointing (Flash and
70 Hogan 1985; Bhushan and Shadmehr 1999; Krakauer et al. 1999; Sabes 2000), or interactions with
71 rigid objects, such as grasping with isometric grip forces (Flanagan and Wing 1997; Fu and Santello
72 2014). The control of “complex objects”, which we define as objects with underactuated internal
73 dynamics, *i.e.* non-rigid objects, has been largely ignored. The few studies that examined the control of
74 complex objects have focused on the two classic control models of balancing a pole and manipulating a
75 linear mass-spring system. For balancing a pole one needs to stabilize an inherently unstable inverted

76 pendulum. Based on kinematic measurements and mathematical modeling, different mechanisms have
77 been suggested, such as intermittent, continuous or predictive control, with forward or inverse models
78 (Mehta and Schaal 2002; Gawthrop et al. 2013; Insperger et al. 2013). Another set of studies on the
79 inverted pendulum system focused on noise and delays to distinguish between the continuous vs.
80 intermittent nature of control (Cluff et al. 2009; Milton 2011; Milton et al. 2013). A linear mass-spring
81 system has served as a model to examine optimization criteria in human control, such as generalized
82 kinematic smoothness (Dingwell et al. 2014), effort and accuracy (Nagengast et al. 2009), or minimum
83 acceleration with constraints on the center of mass (Leib et al. 2012). Two studies compared the
84 contributions of visual and haptic feedback and their results highlighted the essential role of haptic
85 feedback over visual feedback in controlling the object (Huang et al. 2007; Danion et al. 2012). Lastly,
86 another set of studies looked at the compression of a buckling spring, modeling the buckling behavior
87 with a subcritical pitchfork bifurcation of the nonlinear dynamic system, including integration of multi-
88 sensory information with different time delays (Venkadesan et al. 2007; Mosier et al. 2001).

89
90 All these studies examined point-to-point movements, or short sequences of discrete movements, in
91 which the full complexity of the system's dynamics may not yet be fully manifest. A more extended
92 continuous interaction may reveal more of the challenges arising from complex underactuated
93 dynamics. For instance, when a system is near an anti-resonance frequency, its evolution is very
94 sensitive to small changes in the input, rendering the system's behavior chaotic, and essentially
95 unpredictable in the longer term. Such small perturbations readily arise from the fact that human
96 movements are intrinsically variable. This presents a problem for the widely-held assumption that
97 humans rely on internal models of the manipulated object to select and execute a movement policy
98 (Flanagan et al. 2006; Dingwell et al. 2012, Danion et al. 2012). How can humans learn an internal

99 model of a complex underactuated object that has a potentially unpredictable temporal evolution? How
100 can humans control the behavior of such objects? Relying on feedback control is largely insufficient for
101 the manipulation of objects with complex dynamics due to neural transmission delay. Despite these
102 challenges, humans skillfully manipulate complex objects of all degrees of complexity. How humans
103 achieve this is an open question.

104

105 Extending previous work by Sternad and colleagues (Hasson et al. 2012a; Nasserolelami et al. 2014;
106 Sternad and Hasson 2016, Bazzi et al. 2018), this paper investigates continuous manipulation of an
107 underactuated object with nonlinear internal dynamics. The task of moving a bowl-shaped cup with a
108 ball inside was implemented in a virtual environment, using a cart-and-pendulum model to mimic the
109 ball rolling in the moving cup. Notably, one of our previous studies demonstrated that the continuous
110 evolution of this system shows features of deterministic chaos (Nasserolelami et al. 2014). Using
111 mathematical modeling and simulation of the task dynamics, this previous study examined the strategy
112 that humans adopt when manipulating this complex object in continuous rhythmic fashion. Moving at
113 an imposed frequency, participants chose movement amplitudes that made the interaction easier to
114 predict. Counter to expectation, interaction force and smoothness were not minimized.

115

116 The present study examined the same task, but extended the question in two ways. First, rather than
117 imposing a frequency for the oscillatory movement, the present study prescribed the movement
118 amplitude, leaving frequency free to choose. The task of choosing a frequency gave rise to new
119 behaviors and new questions, because the resonance structure of the system may now play a significant
120 role in the choice of strategy. Second, we extended the modeling of human control by including the
121 mechanical impedance of the hand. The previous study on the same system only considered the

122 dynamics of the cart-and-pendulum system (Nasserolelami et al. 2014). However, the object is in
123 continuous interaction with the human, whose neuromechanical properties are likely to influence the
124 cart-and-pendulum dynamics. Therefore, this study introduced a simplified model of hand mechanical
125 impedance interacting with the cart-and-pendulum system.

126

127 Several studies on unconstrained movements have demonstrated that humans tend to move in a way
128 that minimizes physical effort (*e.g.* Alexander 2000; Prilutsky and Zatsiorsky 2002). Extending these
129 findings to the manipulation of complex underactuated objects, our first hypothesis is that humans seek
130 to minimize the effort, or specifically the interaction force (*Hypothesis 1*). We assessed this hypothesis
131 by quantifying the root-mean-squared value of the interaction force between the object and the hand.
132 However, while demonstrated for free movements, this principle may become less prominent when the
133 manipulated object presents additional challenges, specifically when it develops increasingly erratic
134 behavior that becomes hard or impossible to predict. Therefore, we also tested the hypothesis that
135 humans adopt strategies that make the hand-object interaction more predictable (*Hypothesis 2*). When
136 interactions are predictable it is easier for humans to anticipate the object motion and hence the force
137 arising from the object's internal dynamics. Anticipating this "perturbing" force, subjects can directly
138 generate the appropriate interaction force to achieve the desired movement. Conversely, unpredictable
139 object behavior requires continuous correction and adaptation of the hand movement, which may be
140 tiring, both physiologically and cognitively. Predictability of the object dynamics may therefore obviate
141 computational effort and afford simpler internal models to guide feedforward control. We assessed
142 predictability by quantifying mutual information between the hand-cup interaction force and the object
143 kinematics.

144

145 Addressing *Hypotheses 1* and *2* rendered insight into human movement strategies (what do humans
146 optimize), but they did not inform *how* humans achieved these strategies. Such explanation required
147 closer analysis of the object dynamics. Numerous studies on rhythmic movements have provided
148 evidence that resonance properties of the limbs or the object influence behavior. For example, in
149 walking, the preferred stepping frequency maps onto the resonance frequency of the leg modeled as a
150 simple pendulum (Holt et al. 1990). A study of infants in a “jolly jumper” showed that infants tune into
151 the resonance frequency of the jolly jumper (Goldfield et al. 1993). Rhythmically swinging hand-held
152 pendulums of different mass and length has demonstrated that humans have a tendency to oscillate at
153 the natural frequency of the hand-pendulum system (Yu et al. 2003). One main advantage of moving at
154 the resonance frequency is its energetic efficiency: in oscillatory systems at resonance, the ratio
155 between the amplitude of the movement output and the force input is maximal. Another feature of
156 oscillating at resonance has been shown by Goodman et al. (2000) in a study on rhythmic limb
157 movements. Time series analysis using phase space embedding revealed that the trajectories became
158 more predictable when oscillating at resonance. However, that study focused on pendular limb
159 movements, and the applicability of its findings to the manipulation of underactuated objects is unclear.
160 We therefore tested an additional hypothesis that in complex underactuated object control, humans
161 exploit the resonance structure of the manipulated object (*Hypothesis 3*). As the analyses showed, the
162 manipulated object together with the hand not only had one, but two resonance frequencies separated
163 by an anti-resonance frequency, a structure that will aid in interpreting the results.

164

165 In the experiment, participants manipulated a virtual cart-and-pendulum system at their preferred
166 frequency with the movement amplitude prescribed. To evaluate the strategies that humans adopted we
167 mathematically examined the cart-and-pendulum system coupled to a simple model of hand

168 impedance. This model-based analysis allowed us to assess alternative execution strategies, *i.e.*
169 different values of frequency and hand impedance that could be used to perform the task. Interaction
170 forces and the degree of predictability were calculated both experimentally and in simulation.
171 Comparison of human behavior with the mathematically derived results showed that participants did
172 not minimize interaction force, but favored strategies with high predictability. In addition, frequency
173 analysis of the coupled object-hand system showed that the degree of predictability was closely related
174 to the resonance and anti-resonance frequencies of the system.

175

176 **Behavioral Experiment**

177 **Participants**

178 Ten young adults with no self-reported neuromuscular pathology volunteered for the experiment (mean
179 age = 24.3 ± 1.8 yrs). All participants performed the task with their dominant hand. They were naive to
180 the purpose of the study and gave written informed consent before the experiment. All procedures were
181 approved by the Northeastern University Institutional Review Board.

182

183 **The Virtual Task**

184 To test the three hypotheses, a virtual task mimicking the manipulation of a bowl-shaped cup with a
185 ball inside was developed. Importantly, this system is underactuated, since moving the cup causes
186 movements of the ball, which simultaneously exerts forces on the cup: the person moving the cup has
187 to take into account these indirectly-controlled forces to obtain the desired movement of the cup. A
188 simplified model of a cup-and-ball was simulated in a virtual environment with visual and haptic
189 feedback via a robotic manipulandum. Participants were asked to move this virtual cup rhythmically

190 between two specified targets, but were allowed to choose their preferred frequency.

191

192 **The Mechanical Model**

193 Similar to (Hasson et al. 2012a, 2012b; Nasserolelami et al. 2014; Sternad and Hasson 2016), the cup-
 194 and-ball system was modeled as a ball sliding in a semi-circular cup (Fig 1A). The cup motion was
 195 limited to one direction in the horizontal plane, without any friction. Under the assumption that the ball
 196 does not roll, but only slides without friction between the cup and ball, the cup-and-ball system was
 197 mathematically equivalent to an undamped pendulum attached to a moving cart (Fig 1B). The ball
 198 corresponded to the pendulum bob, the cup's horizontal position corresponded to the cart position, and
 199 the arc of the cup corresponded to the pendulum's semi-circular path. With this simple model, the full
 200 dynamics of the task could be computed more easily, without sacrificing the essential elements of the
 201 dynamics: underactuated and nonlinear.

202

203 **Fig 1. Model of the task. A:** Conceptual model of the cup-and-ball system. **B:** Mechanical model of
 204 cup-and-ball dynamics as a cart-and-pendulum system.

205

206 Hence, the equations of the cart-and-pendulum motion are

$$(m_c + m_p) \ddot{X} = m_p d [\dot{\theta}^2 \sin \theta - \ddot{\theta} \cos \theta] + F_{inter} = F_{ball} + F_{inter}$$

207

$$\ddot{\theta} = -\frac{\ddot{X}}{d} \cos \theta - \frac{g}{d} \sin \theta \quad (1)$$

208 where X is the cart position, θ is the pendulum angle, F_{inter} is the force applied by the human on the
 209 cart, and F_{ball} is the force applied by the pendulum (the ball in the conceptual model) on the cart.

210 Parameters of the system are the mass of the cart m_c , mass of the pendulum m_p , the pendulum length d ,

211 and the gravitational acceleration g . The following values were used: $m_c = 2.40$ kg, $m_p = 0.60$ kg, $d =$
212 0.45 m. These values were chosen because they rendered resonance and anti-resonance frequencies of
213 the system that were well within human motor capacities and within reach of participants. The cart and
214 pendulum masses were chosen to make the object light enough to avoid fatigue. The ratio of cart and
215 pendulum masses was set to make the underactuated internal dynamics a prominent feature, *i.e.*
216 participants clearly felt the forces generated by the ball. For lighter ball masses, the cart-and-ball
217 system approximated a rigid object.

218

219 **Apparatus and Data Acquisition**

220 The dynamics of the cup-and-ball system were simulated in a virtual environment (Fig 2). Participants
221 were seated on an adjustable chair in front of a screen and interacted with the virtual environment via a
222 3-degree-of-freedom robotic manipulandum (HapticMaster®, Motekforce, Amsterdam, Netherlands)
223 (Van der Linde and Lammertse 2003). The force applied by the participants on the handle of the
224 robotic arm (F_{inter} in Eq 1) controlled the position of the virtual cup (X in Eq 1). The movements of the
225 robotic arm were restricted to horizontal translations parallel to the participant's frontal plane to ensure
226 a one-dimensional motion of the cup as in the model. Participants felt the interaction force (system
227 inertia and ball force F_{ball} in Eq 1) via the force feedback provided by the robotic manipulandum. A
228 custom-written C++ program based on the HapticAPI (Moog FCS Control Systems) computed the ball
229 kinematics and controlled the virtual display as well as the force feedback.

230

231 **Fig 2. Experimental set-up of the ball-and-cup task using virtual reality and force feedback. A:**
232 Rendering of the task in the virtual environment: the robotic manipulandum provided haptic feedback
233 of the mechanical interaction with the object, while the behavior of the system was displayed online on

234 the back-projection screen. The physical model used the distances shown on the figure, while the
235 distances displayed on the screen were multiplied by a factor of 4 for visibility. The cup displayed was
236 7.5 times smaller than the physical arc determined by the length d of the pendulum. **B:** A participant
237 using the HapticMaster to interact with the simulated cup-and-ball system. The position of the cup was
238 controlled by the position of the end-effector of the robot.

239

240 The cup and ball movements were displayed on a 2.40 m \times 2.40 m back-projection screen located 2.15
241 m in front of the participants. The display consisted of two green rectangular targets on a horizontal
242 line delimiting the displacement of the cup; a yellow semi-circle represented the cup and a small white
243 circle represented the ball (Fig 2). Although the cup was only displayed as a semi-circle, there was no
244 restriction on the ball angle and the pendular rotations could exceed 90° without the ball escaping the
245 cup. The visual translation of the cup was 4.0 times the physical displacement of the manipulandum.
246 The cup displayed on the screen was 7.5 times smaller than the physical dimension of the cup (set by
247 the pendulum length d), in order to have plausible dimensions and fit the display. The force applied by
248 the participants on the robotic arm (F_{inter}), the cup kinematics (position X , velocity \dot{X} , and acceleration
249 \ddot{X}) and the computed ball kinematics (angular position θ , angular velocity $\dot{\theta}$, and angular acceleration $\ddot{\theta}$)
250 were recorded at 120 Hz.

251

252 **Experimental Task and Instructions**

253 Participants were asked to move the cup rhythmically between two targets located at a horizontal
254 distance of 16.5 cm from one another (physical distance between the center of each target, Fig 2A).
255 Participants were instructed to place the cup within the target rectangle at each excursion, so movement
256 amplitude was prescribed. However, the scaled cup was 3 cm wide, while each target was 4.5 cm wide;

257 the peak-to-peak excursion of the physical cup oscillation could therefore range from 15 to 18 cm and
258 still satisfy the task. This tolerance gave participants some leeway to develop their preferred motion.
259 Further, participants were told that they could freely choose their frequency of oscillation and that they
260 could change it throughout the experiment to arrive at their most preferred frequency. Even though
261 participants did not receive explicit restrictions on the movement frequency, a demonstration of the
262 task by the experimenter and the emphasis to “move rhythmically” discouraged them from extremely
263 slow movements. Note that people do not necessarily prefer to move as slowly as possible, even though
264 this may save effort (Van der Wel et al. 2010, Park et al. 2017). No instruction was given regarding the
265 position of the ball within the cup, but participants were informed that the ball could not escape the cup
266 (*i.e.* the behavior was that of a pendulum – attached with a string – rather than that of a loose ball).
267 However, due to the haptic feedback provided by the manipulandum, participants could not ignore the
268 movement of the ball: the ball movement affected the cart movement, as in a real system, and
269 participants felt and saw it. Note that this experimental design intentionally refrained from specifying a
270 single optimal task performance, but rather aimed to give insight into what participants preferred to do,
271 especially after some exploration and practice.

272

273 The experiment consisted of 5 blocks of 10 trials each. Each trial lasted 45 s. The trials within a block
274 were separated by a 15 s pause, and the blocks were separated by a break of several minutes. At the
275 beginning of each trial, the cup was positioned at the center of the left target, and the ball rested at the
276 bottom of the cup.

277

278 **Data Analysis**

279 As the task could be achieved by multiple solutions, *i.e.* it had redundancy, we distinguished between

280 execution and the outcome or result of the movement. Performance was quantified by variables that
281 fully described the kinematics of the system, *i.e.* amplitude and frequency of cart and pendulum, while
282 the outcome was quantified by the task or result variables interaction force, predictability and
283 resonance. Result variables are metrics that explicitly tested the hypotheses.

284

285 **Task Performance and Kinematic Variables:** The task instructions elicited trajectories close to a
286 sinusoid, therefore the movements of the cart (cup) were characterized by the amplitude A_k and the
287 frequency f_k of each cycle k (*i.e.* each back-and-forth movement). The cart amplitude A_k was defined as
288 the half-distance between the minimum and the maximum of the cart position during cycle k . The cart
289 period T_k was defined as the time between two successive maxima of the cart position; the oscillation
290 frequency was $f_k = 1/T_k$. In addition, we quantified the relative phase between the cart and pendulum
291 movements by computing the time lag that maximized the cross-correlation between the time-series of
292 the cart position and pendulum angle. The resulting time lag was then converted into relative phase.

293

294 In order to detect the extrema in the cart position, the difference between successive data points, *i.e.*
295 velocity, was computed. Extrema were detected as those values where the sign changed. In order to
296 ensure robust detection of the cart extrema, the cart position data were smoothed with a zero-phase-lag,
297 fourth-order, low-pass Butterworth filter with a 3 Hz cut-off frequency. Note that this smoothing was
298 used only for detecting the extrema.

299

300 **Result Variables:** *Hypothesis 1 – Minimize Interaction Force:* The net force required to perform the
301 task was estimated by the root mean square of the continuous interaction force $RMSF$

$$RMSF(F_{inter}) = \frac{1}{T} \int_0^T F_{inter}^2(t) dt \quad (2)$$

302 where T is the duration of the trial. Note that this hypothesis is about the hand-cart interaction force and
 303 not the overall force exerted by the participants. In particular, muscular effort was not evaluated.

304

305 *Hypothesis 2 – Maximize Predictability:* Predictability is a mathematical concept that can be
 306 operationalized in several ways. We opted to characterize the degree of predictability of the object
 307 dynamics by the mutual information between the input and the output of the system, *i.e.* the cart
 308 trajectory and the interaction force F_{inter} . Mutual information is an information-theoretic metric that
 309 quantifies the statistical dependency between two variables, and thereby quantifies how much knowing
 310 one of the variables reduces the uncertainty about the other. High mutual information indicates a small
 311 degree of uncertainty (Cover and Thomas 2012). In the present context, mutual information quantifies
 312 the degree to which the long-term evolution of the interaction force can be expected, *i.e.* predicted, if
 313 the cart trajectory is known. Unlike cross-correlation, which is limited to linear relations between
 314 variables, mutual information assesses both linear and nonlinear dependency. It is therefore more
 315 suitable for this nonlinear system. In particular, mutual information has been commonly used to
 316 quantify predictability of weather and climate, which are modeled by chaotic dynamical systems
 317 (DeSole 2004; Kleeman 2011).

318

319 The cart trajectory, which was close to sinusoidal, was represented by its phase in state space $\varphi(t) =$
 320 $\arctan(\dot{X} / (2 f \pi X))$. The interaction force $F_{inter}(t)$ was used as defined above. The predictability
 321 measure MI was therefore

$$MI(\varphi, F_{inter}) = \iint p(\varphi, F_{inter}) \ln \left[\frac{p(\varphi, F_{inter})}{p(\varphi)p(F_{inter})} \right] d\varphi dF_{inter} \quad (3)$$

322 where p denotes the probability density functions for $\varphi(t)$ and $F_{inter}(t)$. Mutual information is a
323 dimensionless quantity, and its unit depends on the base of the logarithm that is used. Here, the natural
324 logarithm was used, and the unit of mutual information is the *nat*.

325

326 *Hypothesis 3 – Exploit Resonance:* Determining the resonance structure of the system requires
327 analytical or numerical analysis of the system dynamics and cannot be inferred from the behavioral
328 data alone. Therefore, *Hypothesis 3* will be addressed later in the modeling and simulation section.

329

330 **Data Processing:** For all kinematic and result variables, only the data between $t = 20$ s and $t = 40$ s of
331 each trial were analyzed to eliminate transients at the beginning and end of the trial. As the
332 experimental data were compared with model simulations described below, trials that significantly
333 deviated from periodicity needed to be excluded as the model assumed periodicity. Hence, when the
334 standard deviation of the oscillation frequency exceeded 10% of its mean, the trial was excluded as this
335 indicated significant deviation from the instructed periodic movements. Similarly, a trial was excluded
336 if the mean cart excursion was smaller than 12 cm or larger than 21 cm, as it did not satisfy the
337 instructed excursion (15 to 18 cm), even allowing an additional 3 cm of tolerance. These relatively
338 stringent inclusion criteria were adopted in post-processing only to enable meaningful comparison with
339 the simulation study reported below (the simulation assumed constant movement frequency within a
340 given amplitude range). They were not success/failure criteria for the participants. One participant's
341 majority of trials did not satisfy these criteria and his entire data were eliminated from subsequent
342 analysis. From the remaining 450 trials of 9 participants, only 17 trials did not meet these criteria.
343 These 17 trials were not at the beginning of the experiment, but distributed across early and late trials.
344 This indicated that the task did not require practice, and performing with periodicity was not a

345 challenge per se.

346

347 The data processing and analyses were performed with MATLAB® (The Mathworks Inc., Natick, MA)
348 and Gnumeric. The numerical values of the interaction force and predictability estimates for each
349 experimental trial were computed with Matlab from the experimental trajectories. Mutual information
350 was calculated with the Matlab MIToolbox-2.1.2. Statistical comparisons were performed using t-tests
351 since the measures were normally distributed (confirmed by Kolmogorov–Smirnov tests).

352

353 **Results**

354 **Task Performance and Kinematic Variables:** As a first overview of participants' performance, Fig 3
355 shows the frequencies f_k adopted by participants plotted as a histogram. To obtain a sufficiently large
356 number of data, each cycle, *i.e.* one back-and-forth movement, was a data point. Two distinct strategies
357 were observed: frequencies were concentrated either between 0.4 and 0.7 Hz (low-frequency strategy)
358 or between 0.9 and 1.8 Hz (high-frequency strategy). The low frequencies were densely concentrated
359 with a sharp peak at around 0.65 Hz, while the higher frequencies were distributed more broadly. These
360 two strategies were separated by a gap between 0.7 and 0.9 Hz: only very few oscillations had a
361 frequency within this range. Four participants adopted the low-frequency strategy, and four participants
362 chose the high-frequency strategy. One participant used low frequencies for the first 35 trials, and then
363 switched to high frequencies; his first 35 trials were therefore put in the low-frequency strategy, and the
364 subsequent trials in the high-frequency strategy. All others were consistent in their choice throughout
365 their 50 trials, excluding the very first trials that were exploration.

366

367 **Fig 3. Distribution of frequencies adopted by all participants when manipulating the virtual cup-**

368 **and-ball system.** The histogram represents the frequencies f_k of every single cycle of the 433 valid
 369 trials (total: 7350 cycles). Note that the x-axis is in log scale.

370

371 Fig 4 depicts a low- and a high-frequency strategy with exemplary time series of the cart and pendulum
 372 positions of two representative participants. For the low-frequency strategy, the cart and pendulum
 373 movements were in-phase (the pendulum's maximum angle was synchronized with the cart's
 374 maximum position). In contrast, the cart and pendulum movements of the high-frequency strategy were
 375 in anti-phase relation (the pendulum maximum angle was synchronized with the cart's minimum
 376 position).

377

378 **Fig 4. Experimental cart and pendulum trajectories.** Representative trajectories of the cart (top
 379 panel) and pendulum (bottom panel) from one participant who chose the low-frequency strategy (**A**)
 380 and one participant who chose the high-frequency strategy (**B**). With the low-frequency strategy the
 381 cart and pendulum movements were in-phase, and the pendulum oscillations were large. With the high-
 382 frequency strategy the cart and pendulum movements were anti-phase and the pendulum oscillations
 383 were smaller.

384

385 Fig 5 shows how the kinematic variables A , f and the relative phase between the cart and pendulum
 386 movements changed over the 50 practice trials for the two groups, *i.e.* two strategies. In overview, all
 387 kinematic variables tended to show an initial transient and then reached a plateau relatively early on.

388

389 **Fig 5. Evolution across trials of the experimental kinematic variables.** **A:** Amplitude A of the cart
 390 oscillations. **B:** Frequency f of the cart oscillations. **C:** Relative phase between the cart movement and

391 the pendulum movement. Note that the amplitude A is defined as the half-distance between the cup
392 extrema. Each of the 433 valid trials was represented by one single value of A , f and $\dot{\theta}_0/\dot{\theta}_{max}$ by
393 averaging across all the cycles within $20 \leq t \leq 40$ s in the trial. The blue and red colors correspond to
394 the two frequency groups. The thick lines denote the mean across participants; the shaded areas denote
395 the standard deviations across participants.

396

397 *Cart Oscillation Amplitude (Fig 5A)*: The amplitude A of the cart was relatively invariant throughout
398 the whole experiment in the low-frequency group, while for the high-frequency group it only stabilized
399 in approximately the last 20 trials. The mean cart amplitude in the last 20 trials converged to similar
400 values in both frequency groups: 8.8 ± 0.1 cm in the low-frequency group and 8.9 ± 0.1 cm in the high-
401 frequency group. These values were within the instructed amplitude range – though close to the higher
402 limit – showing that both participant groups satisfied the task. The mean amplitudes over the last 20
403 trials were not significantly different between groups ($p = 0.47$).

404

405 *Cart Oscillation Frequency (Fig 5B)*: After initial exploration in which all participants adopted
406 relatively low frequencies (around 0.5 Hz in the very first trials), the frequency f stabilized after
407 approximately 15 trials in both groups. The low-frequency group arrived at a mean movement
408 frequency of 0.65 ± 0.01 Hz (average and standard deviations across the last 35 trials). The high-
409 frequency group adopted a mean movement frequency of 1.27 ± 0.04 Hz (average and standard
410 deviations across the last 35 trials), although the variability across participants was much higher, as
411 already indicated by the broad distribution in Fig 3. The mean frequencies over the last 35 trials were
412 significantly different between groups ($p < 0.01$).

413

414 *Cart and Pendulum Synchronization (Fig 5C):* In the low-frequency group, the relative phase between
415 the cart and pendulum movements remained close to zero for all trials, indicating in-phase movements
416 (average relative phase over all trials: 4.92 ± 2.71 degrees). In the high-frequency group, after abruptly
417 transitioning from 0 to 180 degrees in the first 5 trials, relative phase stabilized at around 180 degrees,
418 indicating anti-phase movements (average relative phase over the last 45 trials: 181.9 ± 4.47 degrees).
419 No intermediate relative phase values were observed in any of the experimental trials.

420

421 **Result Variables and Hypothesis Testing:** Fig 6A and C display the evolution of the result variables
422 interaction force *RMSF* and mutual information *MI*, averaged over all participants across trials. The
423 two frequency strategies are again shown separately. Similar to the kinematic variables, there is an
424 initial change leading to a plateau relatively early. To evaluate the hypotheses the initial 5 trials were
425 compared with the final 5 trials.

426

427 **Fig 6. Evolution across trials of the result variables.** Evolution of the experimental (A, C) and
428 simulated (B, D) result variables root mean square interaction force *RMSF* and mutual information *MI*
429 across trials. The experimental variables were computed from the measured time-series. The simulated
430 variables were computed from time-series obtained by simulation of the coupled model (described
431 below). The simulations were run using the experimental values of the cart amplitude and frequency.
432 The solid lines represent the average over all participants in each of the two frequency groups, and the
433 shaded areas represent one standard deviation.

434

435 *Hypothesis 1 – Interaction Force:* The root mean square interaction force *RMSF* increased from $2.57 \pm$
436 0.56 N to 5.49 ± 0.10 N in the low-frequency group, and from 5.48 ± 1.59 N to 9.09 ± 0.38 N in the

437 high-frequency group between early and late trials. The increase was significant in both groups ($p <$
438 0.001). This evolution suggests that participants did not minimize interaction force, counter to
439 *Hypothesis 1*. Instead, with practice they increased the exerted interaction force. Further, 5 out of the 9
440 participants chose the high-frequency strategy which was associated with significantly higher *RMSF*
441 values. If minimization of interaction forces had been the criterion, all participants should have
442 converged to the low-frequency strategy.

443

444 *Hypothesis 2 - Predictability*: Mutual information *MI* between the interaction force and the cart
445 kinematics of the low-frequency group increased from 1.25 ± 0.05 nat in the first 5 trials to 1.44 ± 0.06
446 nat in the last 5 trials. In the high-frequency group, mutual information increased from 1.36 ± 0.08 nat
447 to 1.53 ± 0.03 nat between early and late trials. The increase was significant in both groups ($p < 0.003$)
448 supporting *Hypothesis 2* that participants sought to increase predictability of the system they interacted
449 with. Note that though the increase in *MI* seemed modest, the maximum achievable value of *MI* was
450 around 1.8 nat (for achievable oscillation frequencies). Therefore, the observed relative increases were
451 important.

452

453 **Simulations and Analysis of the Result Space**

454 The results of the behavioral experiment provided support for *Hypothesis 2* that humans strive to
455 increase the predictability of the interaction when manipulating an inherently erratic or unpredictable
456 system. Conversely, the interaction force was not minimized in this interactive task (counter to
457 *Hypothesis 1*). To further evaluate these findings and to test *Hypothesis 3*, we compared the strategies
458 adopted by participants with possible alternative executions to shed light on priorities in human control.
459 To this end, model simulations were performed to compute the result variables for alternative

460 executions that could have achieved the task.

461

462 **A Coupled Model**

463 In a previous study, the task dynamics was analyzed by considering the behavior of the cart-and-
 464 pendulum system alone without including the controlling hand (Nasserolelami et al. 2014). However,
 465 this uncoupled model only partly replicated our experimental data (see Appendix A). We therefore
 466 extended the model to include the continuous coupling between the cart and the hand.

467

468 **Mechanical Model and Forward Dynamics:** To capture the dynamics of the task more accurately, the
 469 cart-and-pendulum system was coupled to the hand dynamics (Fig 7). The hand dynamics was
 470 represented by an ideal force generator (force F_{input}) in parallel with a spring (stiffness K) and a damper
 471 (damping coefficient B). $F_{input}(t)$ was the force required to follow a desired trajectory ($X_{des}(t), \dot{X}_{des}(t)$).
 472 If the full dynamics of the task – including the pendulum force – were perfectly anticipated,
 473 participants would be able to generate an input force F_{input} allowing the cart to exactly follow the
 474 desired trajectory $X_{des}(t)$. In reality, however, it was unlikely that participants learnt the perfect model
 475 due to the pendulum force acting as a perturbation. Therefore the motion due to the generated input
 476 force $F_{input}(t)$ did not exactly track the desired cart trajectory, so that the actual cart trajectory X
 477 differed from X_{des} . The spring and damper – which were a simplified model of hand impedance – then
 478 served to resist this perturbation. Note that this model represented the impedance at the level of the
 479 limb: the stiffness K and damping B corresponded to limb features and not to properties of the involved
 480 muscles. The equations of motion of the coupled model are

$$(m_c + m_p) \ddot{X} = m_p d [\dot{\theta}^2 \sin \theta - \ddot{\theta} \cos \theta] + F_{inter} = F_{ball} + F_{inter}$$

$$\ddot{\theta} = -\frac{\ddot{X}}{d} \cos \theta - \frac{g}{d} \sin \theta \quad (4)$$

$$F_{inter} = F_{input} - K(X - X_{des}) - B(\dot{X} - \dot{X}_{des})$$

481 Given the task instructions, the desired trajectory was a sinusoid $X_{des}(t) = A \sin(2\pi f t + \pi/2)$.

482

483 **Fig 7. Model used to analyze the dynamics of the task in simulation.** Forward dynamics of the cart-
484 and-pendulum system coupled to a model of hand impedance.

485

486 The coupled model was simulated with forward dynamics, *i.e.* computing the system state variables
487 $X(t), \dot{X}(t), \theta(t), \dot{\theta}(t)$ and interaction force $F_{inter}(t)$ from a known $F_{input}(t)$. Since $F_{input}(t)$ could not be
488 measured experimentally, it was chosen to match the force required to manipulate a rigid object of
489 similar mass, *i.e.* $F_{input}(t) = (m_c + m_p) \ddot{X}_{des}(t)$. Humans can manipulate rigid objects very accurately,
490 suggesting that they have a good model of the task dynamics. The hand impedance parameters K and B
491 were considered constant during a trial.

492

493 **Execution Variables:** To evaluate the three hypotheses, one must first define a "strategy": a strategy
494 was defined by the set of execution variables that participants directly controlled and that fully
495 determined the task outcome (and hence referred to as result variables). While the cart oscillation
496 amplitude A was prescribed in the experiment, participants could freely choose three variables of the
497 coupled model: the movement frequency f , the hand stiffness K and the damping B , referred to as
498 execution variables.

499

500 Unlike the movement frequency f , the experimental hand stiffness and damping could not be measured

501 directly, but had to be estimated to afford forward simulations. To this end, an optimization was
502 conducted which aimed to estimate the values of K and B for which the simulated cart and pendulum
503 trajectories best resembled the experimental trajectories. The optimization process and the cost
504 criterion C are detailed in Appendix B.

505

506 **Simulation of Result Variables and Hypothesis Testing:** As for the behavioral experiment, the
507 simulation tested the hypotheses by evaluating the result variables root mean squared interaction force
508 $RMSF$ (Eq. 2) and mutual information MI between the cart kinematics and the interaction force (Eq. 3).
509 To obtain the space of all executions spanned by execution variables f , K and B forward dynamics
510 simulation of the coupled model were run to generate the profiles of the cup kinematics $\varphi(t)$ and the
511 interaction force $F_{inter}(t)$. Using Matlab-Simulink, the simulation time was 45 s, but only data from 20
512 $\leq t \leq 40$ s were analyzed to eliminate transients. The two result variables MI and $RMSF$ were then
513 calculated with Matlab as for the experimental data. These results then served to test *Hypotheses 1* and
514 *2*.

515

516 To evaluate *Hypothesis 3* (exploit resonance), a frequency response analysis of the coupled model was
517 conducted in Matlab. Due to the nonlinearity of the coupled cart-and-pendulum plus human hand
518 system, classic frequency response tools could not be used. However, the system could be linearized
519 assuming small pendulum angles. Although this approximation was not valid for all frequencies, the
520 linear analysis allowed further insight into the behavior of the system. In the frequency response
521 analysis, only one of the execution variables, the movement frequency f , was varied, while the hand
522 stiffness K and damping B were fixed to typical values: one corresponding to the mean values of K and
523 B adopted by participants in the low-frequency group, and the other to the mean values in the high-

524 frequency group (see Appendix B for the identification procedure of experimental values of K and B).

525

526 **Simulation Results of the Coupled Model**

527 Figs 8A and 9A display the 3D execution space spanned by frequency f , stiffness K and damping B . For
 528 each combination or point in this space the result variables $RSMF$ and MI were calculated (resolution of
 529 f : 0.005 Hz, resolution of K : 2 N/m, resolution of B : 1 N.s/m). The green shades denote the area of low
 530 interaction force $RSMF$ (Fig 8A) and the pink shades denote the areas of high MI or predictability (Fig
 531 9A), the hypothesized strategies according to *Hypothesis 1* and 2, respectively. The blue dots are the
 532 participants' data, one point for each trial. Note that the participants' data points in the two figures are
 533 the same to compare them with the two simulated result variables. Figs 8B and 9B show a 2D contour
 534 map of the same $RSMF$ and MI , plotted for a constant value of hand damping $B = 10$ N.s/m. Hence, this
 535 2D space only shows a subset of all participants' data points (for $8 < B < 12$ N.s/m). The result space
 536 for MI contains one area of very low predictability for frequencies around 0.8 Hz (Fig 9). This area
 537 coincides with an area where the interaction force $RSMF$ is low (Fig 8); therefore, the two hypotheses
 538 of interaction force minimization and predictability maximization are mutually exclusive. Conversely,
 539 for frequencies around 0.64 Hz and higher than 1.20 Hz, predictability was high, but interaction force
 540 was high as well.

541

542 **Fig 8. 3D plot and 2D contour map of $RSMF$ in the space of the execution variables. A:** 3D plot of
 543 the root mean square interaction force $RSMF$ in the space spanned by the three execution variables f , K
 544 and B . The green shading represents areas of low interaction force, $RSMF < 3$ N. **B:** 2D map of $RSMF$
 545 in the space spanned by two of the execution variables: f and K . The hand damping B was fixed at 10
 546 N.s/m. The blue dots represent the strategies (f , K , B) adopted by participants in the experiment. The

547 dark blue dots correspond to trials for which the impedance fit was good (cost $C < 0.15$, 80 % of trials);
 548 the lighter dots are trials where $0.15 < C < 0.20$ (12 % of trials). The trials where the impedance fit was
 549 poor ($C > 0.20$) are not represented since they were not reliable (8 % of trials). The cost C is defined in
 550 Appendix B.

551

552 **Fig 9. 3D plots and 2D contour map of MI in the space of the execution variables. A:** 3D plot of
 553 the mutual information MI between the cart trajectory and interaction force in the space spanned by the
 554 three execution variables f , K and B . The pink shading represents areas of high mutual information,
 555 $MI > 1.2$ nat. **B:** 2D map of MI in the space spanned by two of the execution variables: f and K . The
 556 hand damping B was fixed at 10 N.s/m. The blue dots represent the strategies (f, K, B) adopted by
 557 participants in the experiment. The dark blue dots correspond to trials for which the impedance fit was
 558 good (cost $C < 0.15$, 80 % of trials); the lighter dots are trials where $0.15 < C < 0.20$ (12 % of trials).
 559 The trials where the impedance fit was poor ($C > 0.20$) are not represented since they were not reliable
 560 (8 % of trials). The cost C is defined in Appendix B.

561

562 **Hypothesis 1 – Interaction Force:** As seen in Fig 8A, very few experimental trials overlapped with
 563 low $RMSF$ solutions (indicated by green areas) that separated the two frequency groups. Very few trials
 564 were centered in the low interaction force/low predictability area, and two of these data points were
 565 based on only a moderately good impedance fit (light blue dot). The 2D section in Fig 8B shows the
 566 modulation of $RMSF$ for different frequency and stiffness combinations. Notably, the low interaction
 567 force solutions are indicated at movement frequencies lower than 0.5 Hz or between 0.7 and 0.9 Hz.
 568 The experimental data points clearly were not in these regions and therefore did not support *Hypothesis*
 569 *I*.

570

571 In addition, the simulated time series of the model were analyzed in analogous fashion to the
572 experimental time series. The simulated *RMSF* was computed from time-series obtained by simulation
573 of the coupled model initialized with the experimental values of the execution variables. Fig 6B
574 displays the evolution across trials of the simulated *RMSF* averaged over all participants in each of the
575 two frequency groups. The significant increase in *RMSF* from early to late trials in both groups was a
576 further indicator that low interaction force was not a priority. The simulated *RMSF* increased from 2.35
577 ± 0.51 N to 4.89 ± 0.07 N in the low-frequency group and from 4.42 ± 1.89 N to 7.44 ± 0.58 N in the
578 high-frequency group ($p < 0.001$). Note that despite some discrepancies between the experimental and
579 simulated *RMSF*, the general trends in their evolution and even the magnitudes were remarkably
580 similar, supporting the adequacy of the coupled model and the estimated values of *K* and *B*.

581

582 **Hypothesis 2 - Predictability:** According to Fig 9A, none of the participants chose a strategy located
583 in the area of lowest *MI*, or low predictability (non-shaded areas). The two frequency groups were
584 clearly separated by the low *MI* area around 0.8 Hz. Fig 9B details the irregular pattern of *MI* for
585 different frequency-stiffness combinations, with adjacent regions of high and low *MI* between 0.6 and
586 0.8 Hz. This fast change in *MI* was likely due to the resonance structure of the system detailed below.
587 The more intricate variation of *MI* at higher frequencies might be due to chaotic behavior. The data
588 suggest that participants adopted strategies with relatively high *MI* or high predictability.

589

590 Additionally, *MI* was computed from the time series of the simulated data and is presented in Fig 6D.
591 *MI* increased from 1.11 ± 0.05 nat in the early (first 5) trials to 1.30 ± 0.03 nat in the late (last 5) trials
592 in the low-frequency group ($p = 0.003$). In the high-frequency group, the simulated *MI* increased from

593 1.21 ± 0.07 nat to 1.29 ± 0.02 nat ($p = 0.02$). Again, note that the maximum value of MI was about 1.8
 594 nat. Comparing this progression with the experimental values (Fig 6C) shows that both the time course
 595 and the magnitudes of the MI simulated values were close to the experimental values, supporting the
 596 adequacy of the coupled model and the estimated values of stiffness and damping. This simulation
 597 result strengthens the experimental results that predictability was increased with practice.

598

599 **Hypothesis 3 - Resonance:** One essential feature of the task dynamics is its resonance structure: the
 600 coupled system has two resonance peaks and one anti-resonance frequency or dynamic zero between
 601 the two resonance frequencies. Fig 10 displays Bode magnitude and phase plots of the linearized
 602 coupled model for two representative values of hand impedance. System A was simulated with $K = 100$
 603 N/m and $B = 10$ N.s/m, values that were typical for the low-frequency group. System B with $K = 200$
 604 N/m and $B = 15$ N.s/m was typical for the high-frequency group. As the responses of the two systems
 605 reveal, the resonance peaks depend on the values of K and B . The panels for pendulum angle show one
 606 clear resonant peak at 0.68 Hz for system A and at 0.71 Hz for system B.

607

608 Surprisingly at first sight, the second peaks at the higher frequencies are hardly noticeable. This arises
 609 from the fact that the simulation assumed that subjects generated a sinusoidal predictive force $F_{input}(t)$
 610 intended to produce the desired cart motion $X_{des}(t)$. This predictive force was based on an incomplete
 611 model of the object dynamics which considered only its lowest-frequency mode of behavior, *i.e.* as
 612 though the pendulum and the cart moved as one body $F_{input} = (m_c + m_p)\dot{X}_{des}$. This imperfect predictive
 613 force only partially compensated for object dynamics, which was nevertheless sufficient to counteract
 614 the object's resonances, especially at the higher frequencies. Mathematically, the predictive force
 615 introduced complex-valued zeros near the complex-valued poles that describe the high-frequency

616 resonance. These zeros tended to cancel or ‘mask’ the effect of the adjacent poles, converting a sharp
617 resonant peak into a broad region of nearly-constant magnitude (see Footnote 1).

618

619 Importantly, the response of cup displacement for both systems shows a sharp valley, indicating the
620 anti-resonance at 0.74 Hz between the two resonances. Note that the anti-resonance frequency is
621 identical in system A and B, *i.e.* independent of the values of K and B . The phase plots in Fig 10
622 display the relative phase between the input force and the cart movement (red line), and the relative
623 phase between the input force and the pendulum movement (blue line). Comparison between these two
624 curves highlights that for low frequencies the cart and pendulum are in-phase, while for frequencies
625 higher than the anti-resonance frequency, cart and pendulum motions are anti-phase. In addition, the
626 relative phase between the input force and the cart movement (red line) reveals that for frequencies
627 outside the two resonance frequencies, the cart movement is anti-phase with the input force.
628 Conversely, over a small interval between the two resonance frequencies, the relative phase between
629 the input force and the cart movement is changing.

630

631 For comparison of the model’s resonant peaks with the experimental data, the distributions of the
632 observed frequencies in participants are shown in grey (Fig 10). For the low-frequency group (System
633 A) the peak in the distribution is very close to the system’s resonance peak. For the high-frequency
634 group, participants show a very broad distribution that matches with the smeared-out resonance peak of
635 System B. Comparison between Fig 9 and 10 reveals that the two resonance frequencies of the system
636 coincided with areas of high MI . This suggests that the behavior of the system is easily predictable
637 when oscillating at a resonance frequency. Conversely, the anti-resonance frequency coincides with a
638 region of low MI , therefore the behavior of the system is hard to predict when oscillating at or around

639 the anti-resonance frequency. These results are consistent with *Hypothesis 3*.

640

641 **Fig 10: Bode amplitude and phase plots of the linearized coupled model, for different values of**
642 **hand impedance. A:** $K = 100$ N/m and $B = 10$ N.s/m, typical for the low-frequency group. **B:** $K = 200$
643 N/m and $B = 15$ N.s/m, typical for the high-frequency group. Note that the pendulum amplitude plots
644 have different scales in **A** and **B**. The phase plots of the cart and pendulum are superimposed to
645 highlight the synchronization of their movements. For comparison, the grey histogram represents the
646 distribution of frequencies adopted by participants in the experiment (identical to Fig 3). The part of the
647 graph right (resp. left) of the anti-resonance frequency is greyed out because it is not relevant for
648 system A (resp. B) with values of K and B for which the frequency analysis was performed.

649

650

651 **Discussion**

652 This study examined strategies that humans adopt when manipulating objects with underactuated
653 internal dynamics. To date, the majority of research in motor neuroscience has examined unconstrained
654 movements in highly controlled experimental tasks to render interpretable data; only relatively few
655 studies have examined control of complex objects. However, everyday behavior is full of complex
656 manipulations that set humans apart from primates and other animals. The present study focused on
657 continuous physical interaction with a cart-and-pendulum system, representing the simplified dynamics
658 of a moving a cup of coffee. Participants had to move with a prescribed amplitude, but could choose
659 their preferred frequency. Importantly, in continuous interaction with the complex object, the dynamics
660 of this system is underactuated and can exhibit erratic and unpredictable behavior. Such unpredictable
661 dynamics poses significant challenge to any internal model guiding the goal-directed manipulation.

662

663 Using both behavioral data and numerical analysis of the cart-and-pendulum system coupled to a model
664 of hand impedance, we tested three hypotheses: humans minimize the interaction force required to
665 move the system (*Hypothesis 1*); alternatively, they maximize predictability of the system behavior
666 (*Hypothesis 1*); and/or they exploit the resonance structure of the system (*Hypothesis 3*). Interaction
667 force between hand and cart was quantified by its root mean squared value. Predictability was
668 operationalized by the mutual information between the kinematics of the cart and the interaction force.
669 Exploiting resonance was tested by comparing the chosen frequencies with the resonance structure of
670 the system. Results of the experiment showed that participants increased, not decreased, the interaction
671 force (counter to *Hypothesis 1*), while they also increased predictability of the system with practice
672 (consistent with *Hypothesis 2*). Half the participants chose a strategy that had significantly higher
673 interaction forces, while affording similarly high degree of predictability.

674

675 The results of the simulations gave further support that, among alternative strategies (defined by values
676 of movement frequency and hand impedance that humans could adopt), participants chose strategies
677 with high predictability, but not with low interaction force. These results corroborate and generalize
678 those obtained by Nasserolelami et al. (2014) in a similar experiment that prescribed movement
679 frequency, but left amplitude free to choose. In addition, frequency response analysis of the linearized
680 coupled system showed that participants chose movement frequencies close to the resonance
681 frequencies of the system, while avoiding the anti-resonance frequency (consistent with *Hypothesis 3*).
682 These findings demonstrate that predictability is a control priority in complex underactuated object
683 manipulation, which takes precedence over principles such as interaction force minimization. The fact
684 that results support both *Hypothesis 2* and *Hypothesis 3* suggests that predictability may be explained

685 by the resonance structure of the system. Therefore, manipulation of underactuated objects cannot be
686 understood simply by extending principles of free movements or rigid object manipulation;
687 underactuated object manipulation constitutes a different class of tasks with different control
688 challenges.

689

690 **Assumptions of the Coupled Model**

691 To provide an entry to a quantitative understanding of this complex task, an essential element in our
692 approach was simulation of the task dynamics with only minimal assumptions about the controller. We
693 therefore coupled a simplified model of hand impedance to the cart-and-pendulum system. This
694 coupled model approximated the experimental data more accurately than a previous model with the
695 cart-and-pendulum alone (Appendix A). However, as this model went beyond the physics of the task
696 alone and included the human controller, certain assumptions had to be made.

697

698 **Invariance of Input Force:** One first assumption was that the input force (Eq 4) was equal to the force
699 required to move a rigid object of the same mass as the cart-and-pendulum system; further, the
700 amplitude, frequency, and phase of this input force was the same sinusoidal signal during and across
701 trials. While this is a reasonable initial assumption, it is likely that humans learned to adapt their input
702 force, based on the perceived interaction force and/or the cart displacement. As the simulation kept the
703 input force invariant, the desired cart trajectory was not always accurately tracked, especially when the
704 hand impedance was low. A plausible next modeling step would be to modulate the amplitude of the
705 sinusoidal input force based on the difference between the actual and desired cart amplitude. Even
706 though it is relatively straightforward to include such an adaptation of the input force, this would
707 evidently make the model more complex and not necessarily help to understand the data.

708

709 **Invariance of Hand Impedance:** A second simplifying assumption was that the hand impedance was
710 constant throughout one trial. Given the task instruction and the virtual display, the amplitude of the
711 cart movement was the main concern for participants, while the actual trajectory between the two
712 targets was secondary. Therefore, it could be speculated that participants may increase their arm
713 impedance close to the targets to ensure accuracy in the amplitude, but decrease impedance during
714 translation between targets. A sinusoidally changing impedance might therefore better match
715 experimental data. However, as with the modulation of input force, the potential gain in realism would
716 be at the cost of more parameters to identify. Therefore, constant impedance and constant input force is
717 a reasonable compromise between accurate replication of experimental data and transparency of the
718 model.

719

720 **Predictability, Muscular Effort and Antagonist Co-Contraction**

721 The simulations reveal that high predictability and low interaction force are non-overlapping strategies
722 and the data provide evidence that it is predictability that determines the choice of control strategy. The
723 finding that humans do not try to minimize interaction force may seem to run counter to many studies
724 on unconstrained movements that have shown that humans favor energy- or effort-efficient strategies
725 (Nelson 1983; Alexander 2000; Prilutsky and Zatsiorsky 2002). It should be pointed out that our force
726 criterion only quantified the net external force, *i.e.* interaction force. While this external force
727 increased, it might be that higher predictability had a secondary effect on decreasing internal muscular
728 effort: when the system dynamics is erratic, it is difficult to anticipate and preempt the perturbing force
729 of the pendulum by feedforward control. The user may then rely on his/her hand impedance to reject
730 these perturbations and maintain the desired cart trajectory. This requires increasing the impedance

731 through co-activation of antagonist muscles, which results in higher muscular effort without any
732 consequences on the net external force. Conversely, predictable object dynamics may enable
733 participants to anticipate the perturbing interaction force, and thereby reduce effort due to co-
734 contraction. Predictability can therefore afford a way to minimize the overall muscular effort.

735

736 The strongest evidence that force minimization was not an objective was that half of the participants
737 chose the high-frequency strategy associated with higher forces than the low-frequency strategy (Fig
738 6). If effort were the main concern, all participants should have chosen the lower frequency and lower
739 impedance (Appendix B). As mutual information was similar in both frequency groups, the low-
740 frequency solution would have decreased the overall effort and reconciled the predictability and
741 interaction force objectives. However, one point to note is that the task required only relatively low
742 forces, which may be one reason why optimizing effort was not a priority. Testing the same experiment
743 with different masses for the cart-and-pendulum system is a direction for future work.

744

745 **Predictability, Error Correction and Computational Cost**

746 Another factor that may have influenced participants' choices was that the low-frequency strategy was
747 close to the boundary of the low predictability zone (starting around 0.7 Hz in Fig 9), compared to the
748 high-frequency solution that was more robust or tolerant to variation in frequency. With the low-
749 frequency strategy, small variations could easily lead to erratic behavior and perturbations that require
750 correction. If such error corrections were executed by the CNS, then the computational cost would
751 increase. Computational effort has been recognized and included as a cost in several optimization
752 studies (Todorov and Jordan 2002; Ronsse et al. 2010). Yet in these modeling approaches,
753 computational cost terms have remained unspecified placeholders for unaccounted factors contributing

754 to human control choices. A series of studies by Sternad and colleagues have argued that the human
755 controller may exploit the stability properties of a task to avoid computationally expensive corrections
756 (Sternad 2017). Using the task of rhythmically bouncing a ball with a paddle, several experiments
757 provided robust evidence that human subjects learned to attain dynamic stability, such that small errors
758 passively decayed, obviating the need for explicit corrections (Schaal et al. 1996; Sternad et al. 2000;
759 de Rugy et al. 2003). When applying larger perturbations, additional corrections were evidenced,
760 although the signature of dynamic stability was still visible (Siegler et al. 2010; Wei et al. 2007, 2008).
761 In a similar spirit, mathematical and empirical studies of a throwing task showed that humans seek
762 solutions that are tolerant to error and noise, therefore requiring fewer corrections (Sternad et al. 2001,
763 2014; Cohen and Sternad 2009). Predictability of the interactive dynamics of complex object
764 manipulation may again be a manifestation of human controllers seeking to simplify the control task.

765

766 **Resonance/Anti-Resonance Structure, Effort and Predictability**

767 Did participants choose to move at resonance peaks to reduce effort? As Fig 10A showed, participants
768 who moved the cart and pendulum in phase could take advantage of the low-frequency resonance to
769 reduce effort, but had to exert precise control of frequency to avoid the nearby anti-resonance
770 frequency. Participants who chose the anti-phase strategy expended more muscular effort due to the
771 higher frequency of anti-phase motion and to the elevated stiffness and damping they exhibited.
772 However, the anti-phase motion was available over a much broader range of frequencies (Fig 10B) and
773 therefore required much less precise control of frequency. Further, they were far away from the anti-
774 resonance frequency or dynamic zero at 0.74 Hz.

775

776 Did participants prefer certain cup frequencies because they were associated with specific relative

777 phases between the cart and the pendulum movements or between the input force and the cart
778 movement? Several studies on rhythmic bimanual coordination have shown that humans prefer in-
779 phase and anti-phase relations between two limbs over other phase relations (Kelso 1984; Schöner and
780 Kelso 1988; Sternad et al. 1992, 1996). In the present experiment, participants also oscillated the cart
781 either in-phase (at low frequencies) or anti-phase (at high frequencies) with the ball movements and
782 avoided intermediate relative phases at the anti-resonance frequency. However, this observation does
783 not imply that participants chose strategies for their relative phase values. Except at anti-resonance, the
784 task dynamics did not allow other relative phases as the frequency response plots show (Fig 10). The
785 entire frequency range below 0.65 Hz corresponds to in-phase coupling, but participants of the low-
786 frequency group nevertheless all converged to a narrow area of high predictability (Fig 9). Similarly,
787 the high-frequency group favored those subsets of the frequency range with high predictability. In
788 addition, a large set of frequencies outside of the two resonance frequencies correspond to anti-phase
789 coupling between the input force and the cart movement (red line in Fig 10). It is reasonable to think
790 that participants may prefer this anti-phase coupling between what they predict (input force) and what
791 they actually obtain (cart movement) over any other relative phase. Indeed, anti-phase coupling
792 between force and movement is what one gets in the very common situation of manipulating a rigid
793 object. However, if relative phase was the only concern, participants' data points would be spread over
794 all the frequencies with anti-phase coupling, and not grouped over a narrow frequency range. These
795 observations support that potential phase preferences alone do not account for our observations.

796

797 Why did participants avoid the anti-resonance frequency? At anti-resonance, the force generated by the
798 pendulum movement (F_{ball} in Eq 4) exactly opposes the interaction force exerted by the human (F_{inter}
799 in Eq 4), resulting in zero displacement of the cart. In addition, near the anti-resonance frequency the

800 relation between cart motion and input force undergoes a large and rapid, almost discontinuous, phase
801 shift, whereas the relation between pendulum motion and input force does not (phase plot in Fig 10).
802 Around the anti-resonance frequency, the oscillations of the cart and pendulum desynchronize very
803 quickly and small variations result in large changes in the direction of the perturbing force due to
804 pendulum motion. This makes the compensatory input force that should be applied to obtain the desired
805 cart movement hard or impossible to predict. The results clearly showed that subjects consistently
806 avoided the anti-resonance frequency and, implicitly, favored predictability.

807

808 **A Task-Dynamic Approach, Internal Models and Predictability**

809 Most computational studies on movement control start with a hypothesis about the human controller.
810 For example, several studies of the pole-balancing task investigated specific hypotheses about the
811 neural control system, ranging from different control models to the role of noise or sensory feedback
812 (Mehta and Schaal 2002; Venkadesan et al. 2007; Milton 2011; Milton et al. 2013; Gawthrop et al.
813 2013; Insperger et al. 2013). In contrast, our task-dynamic approach shifted the emphasis to first
814 understand the task and its affordance, while minimizing assumptions about human neuromotor control
815 (Sternad 2017). Starting with a mathematical model of the task and analysis of its dynamics, the
816 solution space can be derived and human solutions can be evaluated. To make this mathematical
817 approach transparent a simplified model is advantageous. Here, we reduced the fluid dynamics of the
818 coffee to a single degree of freedom. As with any virtual implementation, this may raise the question
819 whether the problem has become too simple and results will generalize to the real cup of coffee.
820 Recently, two theoretical studies have indeed analyzed the cup of coffee system in its full physical
821 complexity (Mayer & Kretchetnikov 2012, Han 2016). Comparison of these and our studies may reveal
822 the advantages and disadvantages of the realistic versus computationally simplified approach.

823

824 Our task-based approach does not contradict, but complement controller-based approaches. When for
825 example Nagengast et al. (2009) studied optimal control for the manipulation of a virtual mass-spring-
826 damper system, they assumed that participants had complete knowledge of the system dynamics.
827 Similarly, Dingwell et al. (2002, 2004) showed that participants manipulating a linear mass-spring
828 system displayed behavior compatible with learning an internal model of the object dynamics.
829 However, underactuated objects, such as our cup-and-pendulum system pose a significant challenge
830 due to their possibly unpredictable dynamics leading to an apparent absence of correlation between the
831 human action and the resulting behavior of the system. Increasing the predictability of object dynamics
832 might therefore be a way to increase the chance of acquiring an internal model.

833

834 **Footnotes**

835 Footnote 1: With $K = 100$ N/m and $B = 10$ N.s/m, the high-frequency poles are $-1.87 \pm 6.72i$ and the
836 zeros are $-1.67 \pm 5.53i$ (in rad/s). With $K = 200$ N/m and $B = 15$ N.s/m, the high-frequency poles are
837 $-3.06 \pm 8.95i$ and the zeros are $-2.50 \pm 7.77i$ (in Hz).

838

839 **Appendix A: Limitations of a Model without Hand Impedance**

840 In a previous study, the dynamics of the cup-and-ball task was analyzed by looking at the behavior of
841 the cart-and-pendulum system alone without the controlling hand (Nasserolelami et al. 2014). This
842 uncoupled model is depicted in Fig A1 and the motion of the system is described solely by Eq 1. It is
843 straightforward to simulate this uncoupled model using inverse dynamics calculations: if the cart
844 trajectory $X(t)$ and initial conditions of the cart and pendulum ($X_0, \dot{X}_0, \theta_0, \dot{\theta}_0$) are given, the pendulum
845 trajectory $\theta(t)$ and the interaction forces $F_{inter}(t)$ can be computed using Eq 1 and a numerical

846 integration scheme for θ . This uncoupled model has the advantage that it does not require any
847 assumptions about control by the human (contrary to the coupled model). The only assumption is about
848 the movement of the cart, which could reasonably be modeled by a sinusoid $X(t) = A \sin(2\pi f t + \pi/2)$
849 given the task instructions.

850

851 **Fig A1. Model of the dynamics of the task.** Inverse dynamics model of the cart-and-pendulum system
852 alone.

853

854 A first approach used this simple model to analyze the task in this work. In order to test to what degree
855 this model faithfully reproduced human behavior, we ran inverse dynamics simulations to compute $\theta(t)$
856 and $F_{inter}(t)$. A separate simulation was run for each experimental trial based on $X(t)$ and initial
857 conditions taken from experimental values of $(X_0, \dot{X}_0, \theta_0, \dot{\theta}_0)$ and cart amplitude A and frequency f . This
858 afforded direct comparison of the experimental and simulated trajectories of cart and pendulum and the
859 interaction forces. The cart initial conditions X_0 and \dot{X}_0 were fixed by the assumed sinusoidal shape of
860 $X(t)$: $X_0 = A$ and $\dot{X}_0 = 0$. Although all experimental trials started with the same nominal conditions
861 (immobile pendulum at zero angle), trials contained a transient before participants settled onto their
862 approximate steady-state with their chosen frequency. Initial transients were excluded, because the
863 oscillation frequency varied substantially during this stage. Therefore, the values of the amplitude A ,
864 frequency f , and pendulum initial conditions θ_0 and $\dot{\theta}_0$ were the experimental averages across all cycles
865 within $20 \leq t \leq 40$ s, as in the experimental data analysis. The simulated cart, pendulum and force
866 profiles were then compared with the experimental time-series of the corresponding trial. A simulation
867 was run for each of the 433 experimental trials with their respective values.

868

869 Fig A2 displays one representative example of cart and pendulum trajectories $X(t)$ and $\theta(t)$ and the
 870 interaction force $F_{inter}(t)$ from the two frequency strategies. For the high-frequency strategy, all three
 871 simulated time-series (cart position, pendulum angle, interaction force) closely matched their
 872 experimental counterparts. For the low-frequency strategy, the experimental cart trajectory closely
 873 resembled the simulated trajectory, but the pendulum trajectory and the interaction force diverged after
 874 a few cycles. The experimental profiles were close to periodic, whereas the simulated profiles differed
 875 at each oscillation, developing complex, erratic (possibly chaotic) patterns.

876

877 **Fig A2. Comparison of experimental and simulated trajectories and force time-series for the**
 878 **uncoupled model.** Experiment (red) and simulation (blue) profiles of the cart trajectory, pendulum
 879 trajectory and interaction force for one trial of each frequency strategy. Experimental data correspond
 880 to one representative trial in each of the two frequency strategies. Simulation data were computed from
 881 inverse dynamics of the uncoupled model, initialized with the experimental values of A , f , θ_0 and $\dot{\theta}_0$. **A:**
 882 High-frequency strategy ($A = 8.9$ cm, $f = 1.182$ Hz, $\theta_0 = -0.31$ rad, $\dot{\theta}_0 = -0.05$ rad/s). **B:** Low-frequency
 883 strategy ($A = 8.8$ cm, $f = 0.655$ Hz, $\theta_0 = 0.79$ rad, $\dot{\theta}_0 = -0.08$ rad/s).

884

885 To quantify the divergence, the root-mean-square errors (RMS) between the experimental and
 886 simulated trajectories were computed. Table A1 summarizes RMS error for each quantity X , \dot{X} , θ , $\dot{\theta}$ and
 887 F_{inter} , expressed as percent of its respective maximum value in the corresponding experimental trial. In
 888 the high-frequency group, the RMS error was small and fairly consistent across variables (median RMS
 889 error around 10% of the variable maximum experimental value), indicating a reasonably good match
 890 between the experimental and simulated profiles. This uncoupled model was therefore a competent
 891 representation of the cup-and-ball task for the high-frequency strategy. With the low-frequency

892 strategy, however, the RMS error varied greatly and reached up to 30 % of the maximum value for the
 893 experimental pendulum angle and angular velocity (and interaction force to a lesser extent). These
 894 discrepancies between experimental and simulated data demonstrate that the uncoupled model did not
 895 represent the execution strategies adopted by the low-frequency group sufficiently accurately.

896

897 **Table A1. RMS error between experimental and simulated trajectories and force time-series for**
 898 **the uncoupled model.**

	Low-frequency group		High-frequency group	
	Median	IQR	Median	IQR
$\frac{rms(X^e - X^s)}{\ X^e\ _\infty}$	0.10	0.04	0.08	0.02
$\frac{rms(\dot{X}^e - \dot{X}^s)}{\ \dot{X}^e\ _\infty}$	0.13	0.06	0.08	0.03
$\frac{rms(\theta^e - \theta^s)}{\ \theta^e\ _\infty}$	0.29	0.52	0.13	0.09
$\frac{rms(\dot{\theta}^e - \dot{\theta}^s)}{\ \dot{\theta}^e\ _\infty}$	0.31	0.39	0.11	0.07
$\frac{rms(F_{inter}^e - F_{inter}^s)}{\ F_{inter}^e\ _\infty}$	0.22	0.29	0.12	0.04

899

900 Ratio of RMS error between experimental and simulated data normalized by the maximum value for
 901 the cart and pendulum trajectories and interaction force in both subject groups. The simulated data were
 902 obtained from inverse dynamics simulation of the uncoupled model. The median and interquartile

903 range were computed over all 433 valid trials.

904

905 A likely reason for the divergence between experimental and simulated data is the assumption of a
906 perfectly sinusoidal cart trajectory in the simulations, whereas experimental trajectories exhibited small
907 deviations from this ideal shape. Given the sensitivity of the cart-and-pendulum dynamics to initial
908 conditions, small changes in the participant's movement could lead to significant changes in the system
909 evolution. These deviations of the experimental cart trajectories from a perfect sinusoid could have two
910 main causes: the intrinsic variability of human movements, and the perturbations caused by the internal
911 dynamics of the object. The first cause results from the ever-present human variability: even if the
912 object was rigid, or if there were no object at all, humans are unable to repeat the same exact
913 movements. While present in both frequency strategies, this variability could have different
914 consequences, since the sensitivity of the system to initial conditions is not constant.

915

916 The second cause – the perturbation forces created by the pendulum movements – affected the cart
917 trajectory because the human hand is not an ideal position generator. Unexpected pendulum forces
918 disrupted hand and hence cart movement. Though this is again true for both frequency strategies, the
919 cart trajectory was likely less perturbed in the high-frequency strategy, because hand movements were
920 faster, which is often associated with a higher hand impedance; higher impedance would result in better
921 resistance to external perturbations and lower RMS error (Table A1).

922

923 Furthermore, the interaction force F_{inter} results from two different forces (Eq 1): one is the cart-and-
924 pendulum inertial force $F_{inertia} = (m_c + m_p) \ddot{X}$, and the other is the pendulum force F_{ball} . The average
925 ratio between the RMS pendulum force and the RMS inertial force (computed for $20 \leq t \leq 40$ s) was

926 0.70 ± 0.16 in the low-frequency group and 0.32 ± 0.05 in the high-frequency group (averaged across
 927 all trials of all participants in each of the two groups). Relative to the expected force (*i.e.* required to
 928 accelerate the total system inertia, similar to the manipulation of a rigid object), the magnitude of the
 929 unexpected perturbation (the pendulum force) was thus much higher in the low-frequency group and
 930 was therefore less likely to be resisted. Hence, the current study included the effect of hand impedance
 931 on the dynamics of the cart-and-pendulum system.

932

933 **Appendix B: Estimation of Hand Impedance in the Coupled Model**

934 Unlike the movement frequency f , the experimental hand stiffness K and damping B could not be
 935 measured directly, but had to be estimated from the human data. To this end, an optimization was
 936 conducted which aimed at finding the values of K and B for which the simulated cart and pendulum
 937 trajectories most resembled the experimental trajectories. For each combination of K and B a 45 s
 938 forward dynamics simulation of the coupled model was performed and compared with the
 939 corresponding experimental trial. The continuous variations in the cart amplitude and/or frequency in
 940 the experimental trials were evidently not captured in the simulation as constant desired cart
 941 amplitude/frequency was assumed. The simulations used the average experimental values of A and f
 942 across all cycles of the trial ($20 \leq t \leq 40$ s) to define the desired trajectory $X_{des}(t) = A \sin(2 \pi f t + \pi/2)$
 943 and the input force $F_{input}(t) = (m_c + m_p) \ddot{X}_{des}(t)$. However, the average amplitude and frequency were
 944 only representative of the experimental trial if they did not vary significantly throughout the trial. This
 945 motivated the stringent inclusion criteria in the analysis of the behavioral data.

946

947 All combinations of $10 \leq K \leq 350$ N/m (step size 2 N/m) and $3 \leq B \leq 50$ N.s/m (step size 1 N.s/m) were
 948 tested to find the best fit. The difference between the experimental and simulated trajectories was

949 quantified by the cost C of the normalized root mean square errors of the four quantities $X(t)$, $\dot{X}(t)$, $\theta(t)$,
 950 $\dot{\theta}(t)$

$$C = \frac{1}{4} \left[\frac{\text{rms}(X^e - X^s)}{\|X^e\|_\infty} + \frac{\text{rms}(\dot{X}^e - \dot{X}^s)}{\|\dot{X}^e\|_\infty} + \frac{\text{rms}(\theta^e - \theta^s)}{\|\theta^e\|_\infty} + \frac{\text{rms}(\dot{\theta}^e - \dot{\theta}^s)}{\|\dot{\theta}^e\|_\infty} \right] \quad (1)$$

951 where the superscripts s and e stand for *simulation* and *experimental*, respectively. Only the data within
 952 $20 \leq t \leq 40$ s were included to avoid confounding by transients (both for experimental and simulated
 953 trials).

954

955 While the movement frequency f was fixed in the simulations, experimental frequencies were not
 956 exactly constant within trials. Such variations of the experimental frequency created a temporal offset
 957 between the experimental and simulated trajectories, which could lead to high RMS errors even when
 958 the two profiles were similar. To limit this artifact, C was computed cycle by cycle, *i.e.* the RMS errors
 959 were computed for each cycle k by time-aligning the experimental and simulated trajectories of cycle k .
 960 Subsequently, they were averaged over all cycles.

961

962 Across all trials, the median cost C measured for the best impedance fit of each trial was 0.104 with an
 963 interquartile range of 0.051. Table B1 gives the ratio between the RMS error between experimental and
 964 simulated time-series and the maximum experimental value of the corresponding trial for the state
 965 variables $(X, \dot{X}, \theta, \dot{\theta})$ as well as for the interaction force F_{inter} . The median value of the RMS error was
 966 between 9 and 13% of the maximum value, depending on the variable. Importantly, the error was
 967 consistently low in both groups, unlike for the uncoupled model above (see Table A1 in Appendix A).

968

969 **Table B1: RMS error between experimental and simulated trajectories and force time-series for**

970 **the coupled model.**

	Low-frequency group		High-frequency group	
	Median	IQR	Median	IQR
$\frac{rms(X^e - X^s)}{\ X^e\ _\infty}$	0.09	0.04	0.09	0.02
$\frac{rms(\dot{X}^e - \dot{X}^s)}{\ \dot{X}^e\ _\infty}$	0.11	0.05	0.08	0.03
$\frac{rms(\theta^e - \theta^s)}{\ \theta^e\ _\infty}$	0.11	0.07	0.12	0.07
$\frac{rms(\dot{\theta}^e - \dot{\theta}^s)}{\ \dot{\theta}^e\ _\infty}$	0.12	0.07	0.10	0.05
$\frac{rms(F_{inter}^e - F_{inter}^s)}{\ F_{inter}^e\ _\infty}$	0.13	0.05	0.13	0.04

971

972 Ratio between root mean square error RMS between experimental and simulated data and the
 973 maximum value for the cart and pendulum trajectories and interaction force. The results are separated
 974 for the two frequency groups. The simulated data were obtained with forward simulation of the coupled
 975 model, using the optimized values of K and B for each trial (*i.e.* the values for which the cost C was
 976 minimum).

977

978 The values of hand impedance were different between groups. The comparison of stiffness and
 979 damping values between the two frequency groups was performed with a Wilcoxon signed rank test
 980 because the data were not normally distributed. Both the stiffness K and damping B were significantly
 981 lower in the low-frequency group, with $p = 10e-10$ and $p = 10e-13$ respectively. This is consistent with

982 the known fact that, for a similar task accuracy, limb stiffness usually increases with movement speed.

983

984 These results are the basis for characterizing experimental trials with hand impedance. The coupled
985 model with optimized K and B reproduced experimental trajectory and force time-series much more
986 accurately than the uncoupled model (especially for the low-frequency group), thus confirming its
987 better competence to analyze the experimental task.

988

989

990 **Acknowledgments**

991 The authors wish to thank Fei Ye for her help with the data collection and first analysis.

992

993 **Grants**

994 Dagmar Sternad was supported by the National Institutes of Health R01-HD087089, R01-HD081346,
995 and R21-DC013095 and the National Science Foundation NSF-NRI 1637854 and NSF-EAGER-
996 1548514. Neville Hogan was supported by NIH R01-HD087089, NSF-NRI 1637814, NSF-EAGER-
997 1548501 and by the Eric P. and Evelyn E. Newman fund. Pauline Maurice was supported in part by the
998 European Union's Horizon 2020 Research and Innovation Program under Grant Agreement No.
999 731540.

1000 **References**

- 1001 1. **Alexander R.M.** Energy-minimizing choices of muscles and patterns of movement. *Motor Control*.
1002 2000; 4(1):45–47.
- 1003
- 1004 2. **Bazzi, S., Ebert, J., Hogan, N., Sternad, D.** Stability and Predictability in Dynamically Complex
1005 Physical Interactions. *IEEE International Conference on Robotics and Automation (ICRA)* 2018.
- 1006
- 1007 3. **Bhushan N., Shadmehr R.** Computational nature of human adaptive control during learning of
1008 reaching movements in force fields. *Biological Cybernetics*. 1999; 81(1):39–60.
- 1009
- 1010 4. **Cluff T., Riley M.A., Balasubramaniam R.** Dynamical structure of hand trajectories during pole
1011 balancing. *Neuroscience Letters*. 2009; 464(2):88–92.
- 1012
- 1013 5. **Cohen, R. G., & Sternad, D.** (2009). Variability in motor learning: relocating, channeling and
1014 reducing noise. *Experimental brain research*, 193(1), 69-83.
- 1015
- 1016 6. **Cover T.M., Thomas J.A.** *Elements of information theory*. John Wiley & Sons. 2012,
- 1017
- 1018 7. **DelSole, T.** Predictability and information theory. Part I: Measures of predictability. *Journal of the*
1019 *Atmospheric Sciences*, 2004; 61(20), 2425-2440.
- 1020
- 1021 8. **de Rugy, A., Wei, K., Müller, H., & Sternad, D.** Actively tracking ‘passive’ stability in a ball
1022 bouncing task. *Brain Research*, 2003; 982(1), 64-78.

1023

1024 9. **Danion, F., Diamond, J. S., & Flanagan, J. R.** The role of haptic feedback when manipulating
1025 nonrigid objects. *Journal of neurophysiology*, 2012; 107(1), 433-441.

1026

1027 10. **Dingwell J.B., Mah C.D., Mussa-Ivaldi F.A.** Manipulating objects with internal degrees of
1028 freedom: evidence for model-based control. *Journal of Neurophysiology*. 2002; 88(1):222–235.

1029

1030 11. **Dingwell J.B., Mah C.D., Mussa-Ivaldi F.A.** Experimentally confirmed mathematical model for
1031 human control of a non-rigid object. *Journal of Neurophysiology*. 2004; 91(3):1158–1170.

1032

1033 12. **Flanagan J.R., Bowman M.C., Johansson R.S.** Control strategies in object manipulation tasks.
1034 *Current Opinion in Neurobiology*. 2006; 16(6):650–659.

1035

1036 13. **Flanagan J.R., Wing A.M.** The role of internal models in motion planning and control: evidence
1037 from grip force adjustments during movements of hand-held loads. *The Journal of Neuroscience*, 1997;
1038 17(4):1519–1528.

1039

1040 14. **Flash T., Hogan N.** The coordination of arm movements: an experimentally confirmed
1041 mathematical model. *The Journal of Neuroscience*. 1985; 5(7):1688–1703.

1042

1043 15. **Fu Q., Santello M.** Coordination between digit forces and positions: interactions between
1044 anticipatory and feedback control. *Journal of Neurophysiology*. 2014; 111(7):1519–1528.

1045

- 1046 16. **Gawthrop P., Lee K.Y., Halaki M., O'Dwyer N.** Human stick balancing: an intermittent control
1047 explanation. *Biological Cybernetics*. 2013; 107(6):637–652.
1048
- 1049 17. **Goldfield, E. C., Kay, B. A., & Warren, W. H.** Infant bouncing: The assembly and tuning of
1050 action systems. *Child Development*, 1993; 64(4), 1128-1142.
1051
- 1052 18. **Goodman L., Riley M.A., Mitra S., Turvey M.T.** Advantages of rhythmic movements at
1053 resonance: minimal active degrees of freedom, minimal noise, and maximal predictability. *Journal of*
1054 *Motor Behavior*. 2000; 32(1):3–8.
1055
- 1056 19. **Hasson C.J., Hogan N., Sternad D.** Human control of dynamically complex objects. In: 2012 4th
1057 *IEEE RAS & EMBS International Conference on Biomedical Robotics and Biomechatronics (BioRob)*.
1058 IEEE; 2012a. p. 1235–1240.
1059
- 1060 20. **Hasson C.J., Shen T., Sternad D.** Energy margins in dynamic object manipulation. *Journal of*
1061 *Neurophysiology*. 2012b; 108(5):1349–1365.
1062
- 1063 21. **Holt, K. G., Hamill, J., & Andres, R. O.** The force-driven harmonic oscillator as a model for
1064 human locomotion. *Human Movement Science*. 1990; 9(1), 55-68.
1065
- 1066 22. **Han, J.** A Study on the Coffee Spilling Phenomena in the Low Impulse Regime. *Achievements in*
1067 *the Life Sciences*, 2016; 10(1), 87-101.
1068

- 1069 23. **Huang, F. C., Gillespie, R. B., & Kuo, A. D.** Visual and haptic feedback contribute to tuning and
1070 online control during object manipulation. *Journal of motor behavior*, 2007; 39(3), 179-193.
1071
- 1072 24. **Insperger T., Milton J., Stépán G.** Acceleration feedback improves balancing against reflex
1073 delay. *Journal of the Royal Society Interface*. 2013; 10(79):20120763.
1074
- 1075 25. **Kelso, J. A.** Phase transitions and critical behavior in human bimanual coordination. *American*
1076 *Journal of Physiology-Regulatory, Integrative and Comparative Physiology*, 1984, 246(6), R1000-
1077 1004.
1078
- 1079 26. **Kleeman, R.** Information theory and dynamical system predictability. *Entropy*. 2011; 13(3), 612-
1080 649.
1081
- 1082 27. **Krakauer J.W., Ghilardi M.F., Ghez C.** Independent learning of internal models for kinematic
1083 and dynamic control of reaching. *Nature Neuroscience*. 1999; 2(11):1026–1031.
1084
- 1085 28. **Leib R., Karniel A.** Minimum acceleration with constraints of center of mass: a unified model for
1086 arm movements and object manipulation. *Journal of Neurophysiology*. 2012; 108(6):1646–1655.
1087
- 1088 29. **Mayer, H. C., & Krechetnikov, R.** Walking with coffee: Why does it spill?. *Physical Review E*,
1089 2012; 85(4), 046117.
1090
- 1091 30. **Mehta B., Schaal S.** Forward models in visuomotor control. *Journal of Neurophysiology*. 2002;

1092 88(2):942–95

1093

1094 31. **Milton J.G.** The delayed and noisy nervous system: implications for neural control. *Journal of*
1095 *Neural Engineering*. 2011; 8(6):065005.

1096

1097 32. **Milton J.G., Fuerte A., Bélair C., Lippai J., Kamimura A., Ohira T.** Delayed pursuit-escape as
1098 a model for virtual stick balancing. *Nonlinear Theory and its Applications*, IEICE. 2013; 4(2):129–137.

1099

1100 33. **Mosier, K., Lau, C., Wang, Y., Venkadesan, M., & Valero-Cuevas, F. J.** Controlling
1101 instabilities in manipulation requires specific cortical-striatal-cerebellar networks. *Journal of*
1102 *Neurophysiology*. 2011; 105(3), 1295-1305.

1103

1104 34. **Nagengast A.J., Braun D.A., Wolpert D.M.** Optimal control predicts human performance on
1105 objects with internal degrees of freedom. *PLoS Computational Biology* 2009; 5(6):e1000419.

1106

1107 35. **Nasserolelami B., Hasson C.J., Sternad D.** Rhythmic manipulation of objects with complex
1108 dynamics: predictability over chaos. *PLoS Computational Biology*, 2014; 10(10):e1003900.

1109

1110 36. **Nelson, W. L.** Physical principles for economies of skilled movements. *Biological Cybernetics*.
1111 1983; 46(2), 135-147.

1112

1113 37. **Park, S.W., Marino, H., Charles, S. Sternad, D., & Hogan, N.** Moving slowly is hard for
1114 humans: Limitations of dynamic primitives. *Journal of Neurophysiology*. 2017; 118, 1, 69-83.

1115

1116 38. **Prilutsky B.I., Zatsiorsky V.M.** Optimization-based models of muscle coordination. *Exercise and*
1117 *Sport Science Reviews*. 2002; 30(1):32.

1118

1119 39. **Ronsse R., Wei, K., & Sternad, D.** Optimal control of a hybrid rhythmic-discrete task: the
1120 bouncing ball revisited. *Journal of Neurophysiology*. 2010; 103(5), 2482-2493.

1121

1122 40. **Sabes P.N.** The planning and control of reaching movements. *Current Opinion in Neurobiology*.
1123 2000; 10(6):740–746.

1124

1125 41. **Schaal S., Atkeson C.G., & Sternad D.** One-handed juggling: A dynamical approach to a
1126 rhythmic task. *Journal of Motor Behavior*, 1996, 28(2), 165–183.

1127

1128 42. **Schöner G., Kelso J.A.** A synthetic theory of environmentally-specified and learned patterns of
1129 movement coordination. *Biological Cybernetics*, 1988, 58(2), 71-80.

1130

1131 43. **Siegler, I. A., Bardy, B. G., & Warren, W. H.** Passive vs. active control of rhythmic ball
1132 bouncing: the role of visual information. *Journal of Experimental Psychology: Human Perception and*
1133 *Performance*. 2010; 36(3), 729.

1134

1135 44. **Sternad, D.** Control of intermittent and continuous objects. In J.-P. Laumond, *Geometric and*
1136 *Numerical Foundations of Movement*, New York: Springer. 2017; 301–338,

1137

1138 45. **Sternad D., Abe M.O., Hu X., & Muller H.** Neuromotor noise, sensitivity to error and signal;-
1139 dependent noise in trial-to-trial learning. *PloS Computational Biology*, 2001, 7, e1002159.

1140

1141 46. **Sternad D., Amazeen E. L., Turvey M. T.** Diffusive, synaptic and synergetic coupling: An
1142 evaluation through in-phase and antiphase rhythmic movements. *Journal of Motor Behavior*, 1996,
1143 28(3), 255–269.

1144

1145 47. **Sternad D., Duarte, M., Katsumata, H., & Schaal, S.** Dynamics of a bouncing ball in human
1146 performance. *Physical Review E*, 2000, 63(1), 011902.

1147

1148 48. **Sternad D., Hasson, C.J.** Predictability and robustness in the manipulation of dynamically
1149 complex objects. *Progress in Motor Control*. New York: Springer. 2016; 55–77.

1150

1151 49. **Sternad D., Huber, M. E., & Kuznetsov, N.** Acquisition of novel and complex motor skills:
1152 stable solutions where intrinsic noise matters less. *Advances in Experimental Medicine and Biology*,
1153 2014; 826, 101-24.

1154

1155 50. **Sternad D., Turvey M. T., Schmidt R. C.** Average phase difference theory and 1:1 phase
1156 entrainment in interlimb coordination. *Biological Cybernetics*, 1992, 67(3), 223–321.

1157

1158 51. **Todorov, E., & Jordan, M. I.** Optimal feedback control as a theory of motor coordination. *Nature*

1159 *Neuroscience*. 2002; 5(11), 1226-1235.

1160

1161 52. **Van der Linde R.Q., Lammertse P.** HapticMaster-a generic force controlled robot for human
1162 interaction. *Industrial Robot: An International Journal*. 2003; 30(6):515–524.

1163

1164 53. **Van der Wel, R.P.R.D., Sternad, D., & Rosenbaum, D.A.** Moving the arm at different rates:
1165 Slow movements are avoided. *Journal of Motor Behavior*, 2010; 42, 1, 29-36.

1166

1167 54. **Venkadesan M., Guckenheimer J., Valero-Cuevas F.J.** Manipulating the edge of instability.
1168 *Journal of Biomechanics*. 2007; 40(8):1653–1661.

1169

1170 55. **Wei, K., Dijkstra, T.M.H., & Sternad, D.** Passive stability and active control in a rhythmic task.
1171 *Journal of Neurophysiology*. 2007; 98, 5, 2633-2646.

1172

1173 56. **Wei, K., Dijkstra, T.M.H., & Sternad, D.** Stability and variability: Indicators for passive stability
1174 and active control in a rhythmic task. *Journal of Neurophysiology*. 2008; 99, 3027-3041.

1175

1176 57. **Yu, H., Russell, D. M., & Sternad, D.** Task-effector asymmetries in a rhythmic continuation task.
1177 *Journal of Experimental Psychology: Human Perception and Performance*. 2003; 29(3), 616.

1178

1179

1180

1181

1182

1183 **Figures captions**

1184

1185 **Fig 1. Model of the task. A:** Conceptual model of the cup-and-ball system. **B:** Mechanical model of
1186 cup-and-ball dynamics as a cart-and-pendulum system.

1187

1188 **Fig 2. Experimental set-up of the ball-and-cup task using virtual reality and force feedback. A:**

1189 Rendering of the task in the virtual environment: the robotic manipulandum provided haptic feedback
1190 of the mechanical interaction with the object, while the behavior of the system was displayed online on
1191 the back-projection screen. The physical model used the distances shown on the figure, while the
1192 distances displayed on the screen were multiplied by a factor of 4 for visibility. The cup displayed was
1193 7.5 times smaller than the physical arc determined by the length of the pendulum. **B:** A participant
1194 using the HapticMaster to interact with the simulated cup-and-ball system. The position of the cup was
1195 controlled by the position of the end-effector of the robot.

1196

1197 **Fig 3. Distribution of frequencies adopted by all participants when manipulating the virtual cup-**

1198 **and-ball system.** The histogram represents the frequencies f_k of every single cycle of the 433 valid
1199 trials (total: 7350 cycles). Note that the x-axis is in log scale.

1200

1201 **Fig 4. Experimental cart and pendulum trajectories.** Representative trajectories of the cart (top

1202 panel) and pendulum (bottom panel) from one participant who chose the low-frequency strategy (**A**)

1203 and one participant who chose the high-frequency strategy (**B**). With the low-frequency strategy the

1204 cart and pendulum movements were in-phase, and the pendulum oscillations were large. With the high-

1205 frequency strategy the cart and pendulum movements were anti-phase and the pendulum oscillations
 1206 were smaller.

1207

1208 **Fig 5. Evolution across trials of the experimental kinematic variables.** **A:** Amplitude A of the cart
 1209 oscillations. **B:** Frequency f of the cart oscillations. **C:** Relative phase between the cart movement and
 1210 the pendulum movement. Note that the amplitude A is defined as the half-distance between the cup
 1211 extrema. Each of the 433 valid trials was represented by one single value of A , f and $\dot{\theta}_0/\dot{\theta}_{max}$ by
 1212 averaging across all the cycles within $20 \leq t \leq 40$ s in the trial. The blue and red colors correspond to
 1213 the two frequency groups. The thick lines denote the mean across participants; the shaded areas denote
 1214 the standard deviations across participants.

1215

1216 **Fig 6. Evolution across trials of the result variables.** Evolution of the experimental (**A, C**) and
 1217 simulated (**B, D**) result variables root mean square interaction force $RMSF$ and mutual information MI
 1218 across trials. The experimental variables were computed from the measured time-series. The simulated
 1219 variables were computed from time-series obtained by simulation of the coupled model (described
 1220 below). The simulations were run using the experimental values of the cart amplitude and frequency.
 1221 The solid lines represent the average over all participants in each of the two frequency groups, and the
 1222 shaded areas represent one standard deviation.

1223

1224 **Fig 7. Model used to analyze the dynamics of the task in simulation.** Forward dynamics of the cart-
 1225 and-pendulum system coupled to a model of hand impedance.

1226

1227 **Fig 8. 3D plot and 2D contour map of $RMSF$ in the space of the execution variables.** **A:** 3D plot of

1228 the root mean square interaction force $RMSF$ in the space spanned by the three execution variables f , K
 1229 and B . The green shading represents areas of low interaction force, $RMSF < 3$ N. **B**: 2D map of $RMSF$
 1230 in the space spanned by two of the execution variables: f and K . The hand damping B was fixed at 10
 1231 N.s/m. The blue dots represent the strategies (f, K, B) adopted by participants in the experiment. The
 1232 dark blue dots correspond to trials for which the impedance fit was good (cost $C < 0.15$, 80 % of trials);
 1233 the lighter dots are trials where $0.15 < C < 0.20$ (12 % of trials). The trials where the impedance fit was
 1234 poor ($C > 0.20$) are not represented since they were not reliable (8 % of trials). The cost C is defined in
 1235 Appendix B.

1236

1237 **Fig 9. 3D plots and 2D contour map of MI in the space of the execution variables.** **A**: 3D plot of
 1238 the mutual information MI between the cart trajectory and interaction force in the space spanned by the
 1239 three execution variables f , K and B . The pink shading represents areas of high mutual information,
 1240 $MI > 1.2$ nat. **B**: 2D map of MI in the space spanned by two of the execution variables: f and K . The
 1241 hand damping B was fixed at 10 N.s/m. The blue dots represent the strategies (f, K, B) adopted by
 1242 participants in the experiment. The dark blue dots correspond to trials for which the impedance fit was
 1243 good (cost $C < 0.15$, 80 % of trials); the lighter dots are trials where $0.15 < C < 0.20$ (12 % of trials).
 1244 The trials where the impedance fit was poor ($C > 0.20$) are not represented since they were not reliable
 1245 (8 % of trials). The cost C is defined in Appendix B.

1246

1247 **Fig 10: Bode amplitude and phase plots of the linearized coupled model, for different values of**
 1248 **hand impedance.** **A**: $K = 100$ N/m and $B = 10$ N.s/m, typical for the low-frequency group. **B**: $K = 200$
 1249 N/m and $B = 15$ N.s/m, typical for the high-frequency group. Note that the pendulum amplitude plots
 1250 have different scales in **A** and **B**. The phase plots of the cart and pendulum are superimposed to

1251 highlight the synchronization of their movements. For comparison, the grey histogram represents the
1252 distribution of frequencies adopted by participants in the experiment (identical to Fig 3). The part of the
1253 graph right (resp. left) of the anti-resonance frequency is greyed out because it is not relevant for
1254 system A (resp. B) with values of K and B for which the frequency analysis was performed.

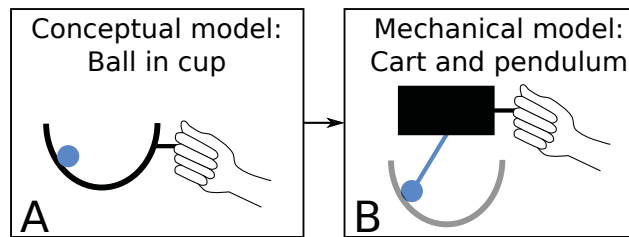
1255

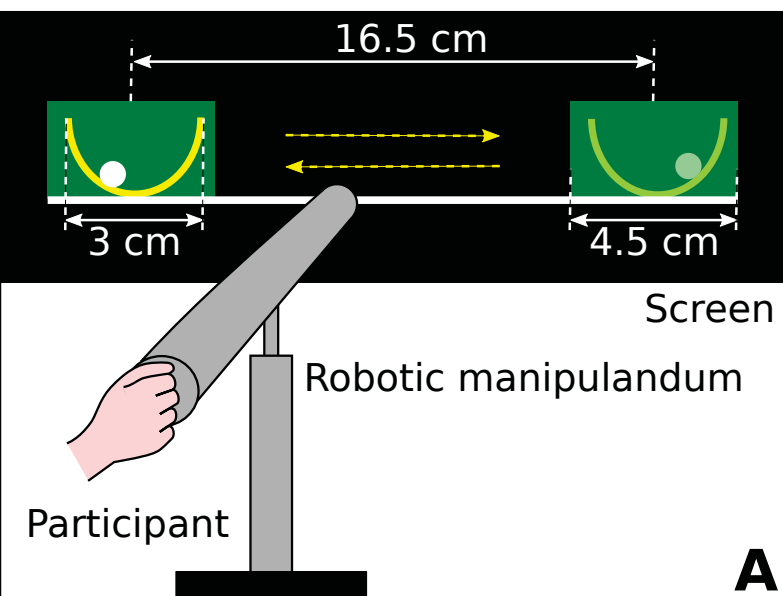
1256 **Fig A1. Model of the dynamics of the task.** Inverse dynamics model of the cart-and-pendulum system
1257 alone.

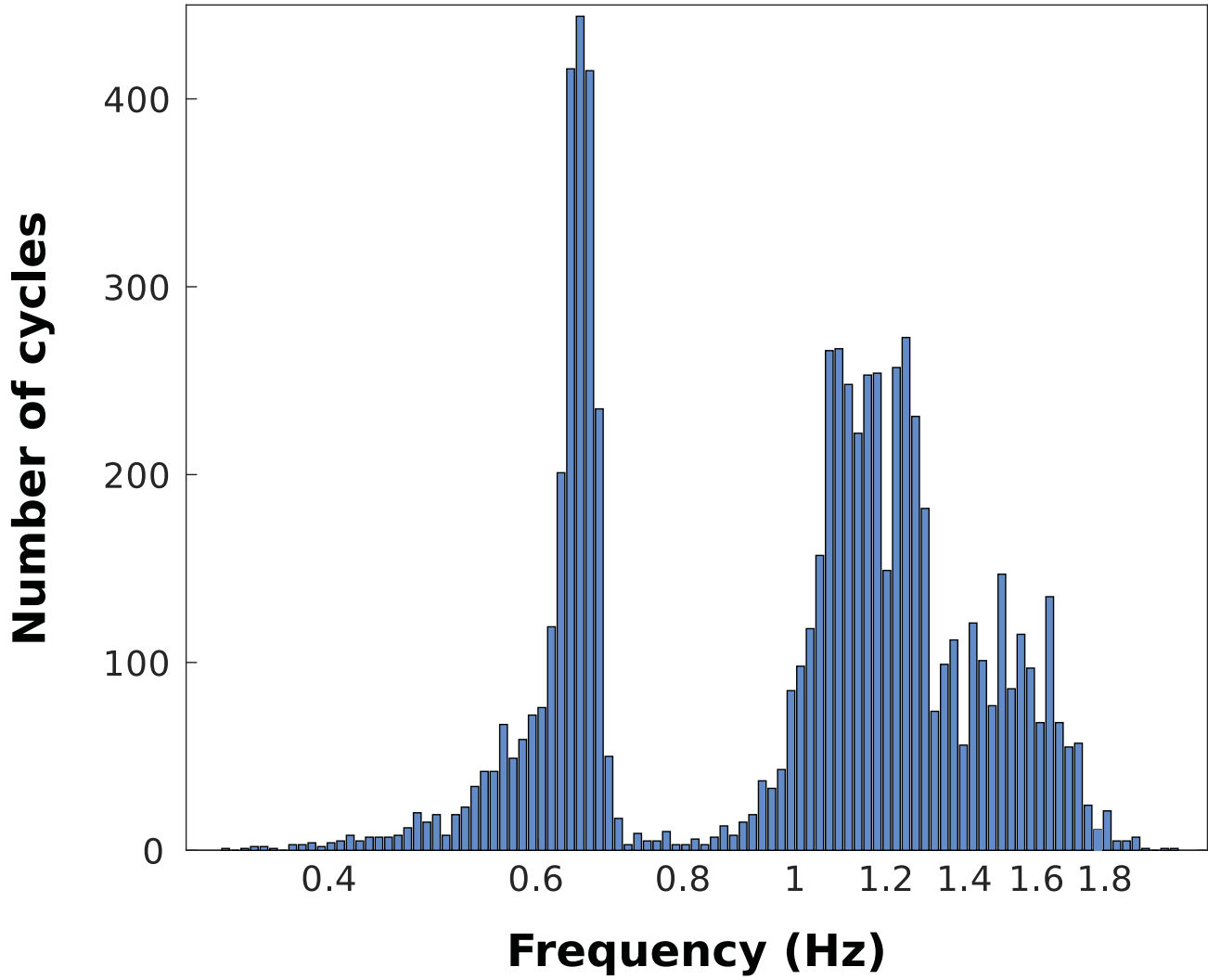
1258

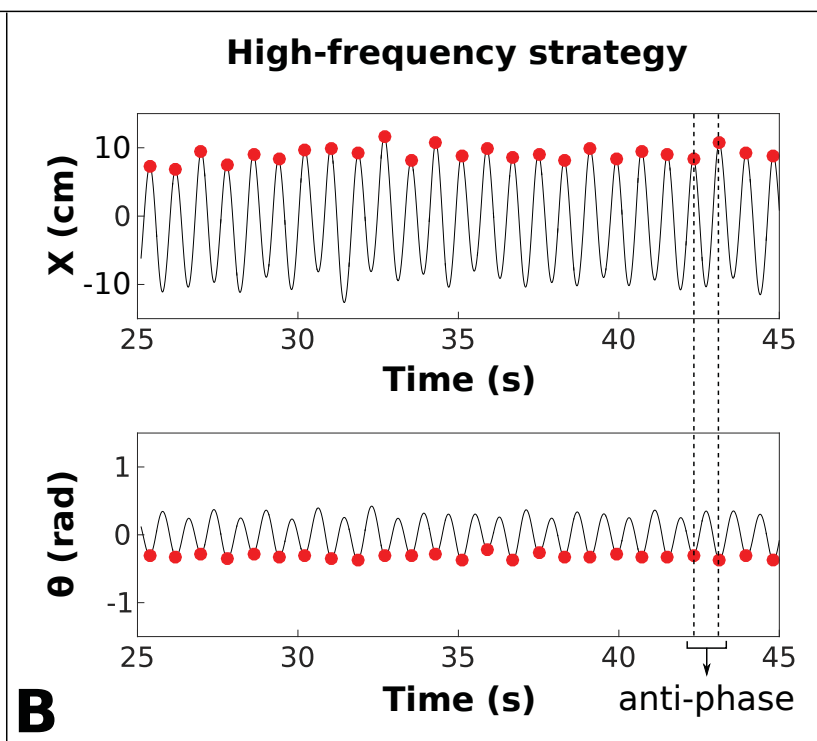
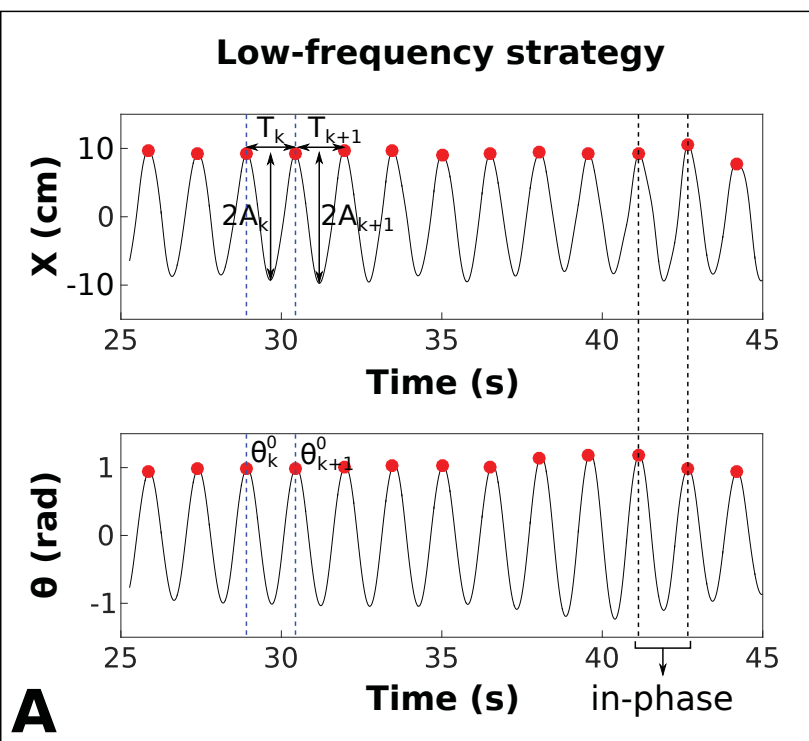
1259 **Fig A2. Comparison of experimental and simulated trajectories and force time-series for the**
1260 **uncoupled model.** Experiment (red) and simulation (blue) profiles of the cart trajectory, pendulum
1261 trajectory and interaction force for one trial of each frequency strategy. Experimental data correspond
1262 to one representative trial in each of the two frequency strategies. Simulation data were computed from
1263 inverse dynamics of the uncoupled model, initialized with the experimental values of A , f , θ_0 and $\dot{\theta}_0$. **A:**
1264 High-frequency strategy ($A = 8.9$ cm, $f = 1.182$ Hz, $\theta_0 = -0.31$ rad, $\dot{\theta}_0 = -0.05$ rad/s). **B:** Low-frequency
1265 strategy ($A = 8.8$ cm, $f = 0.655$ Hz, $\theta_0 = 0.79$ rad, $\dot{\theta}_0 = -0.08$ rad/s).

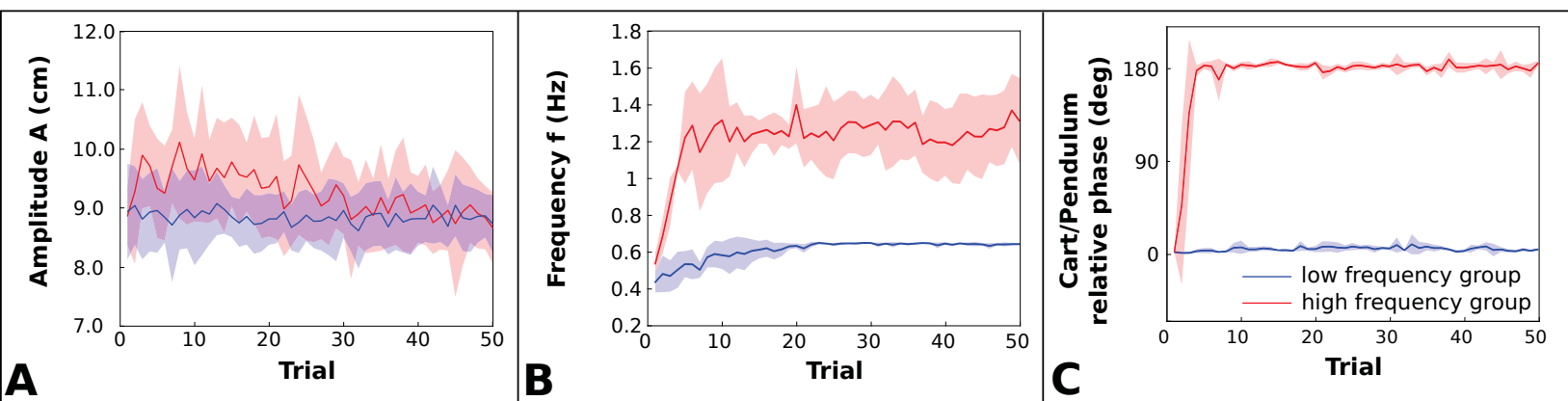
1266





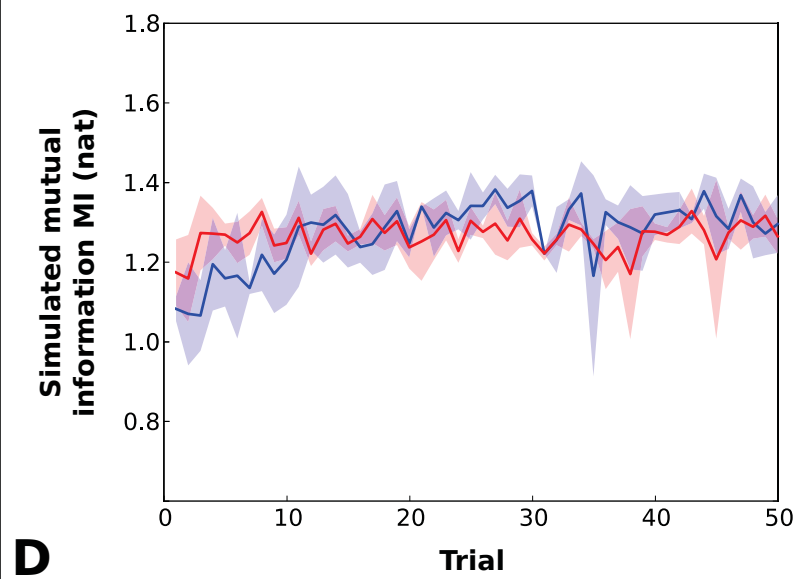
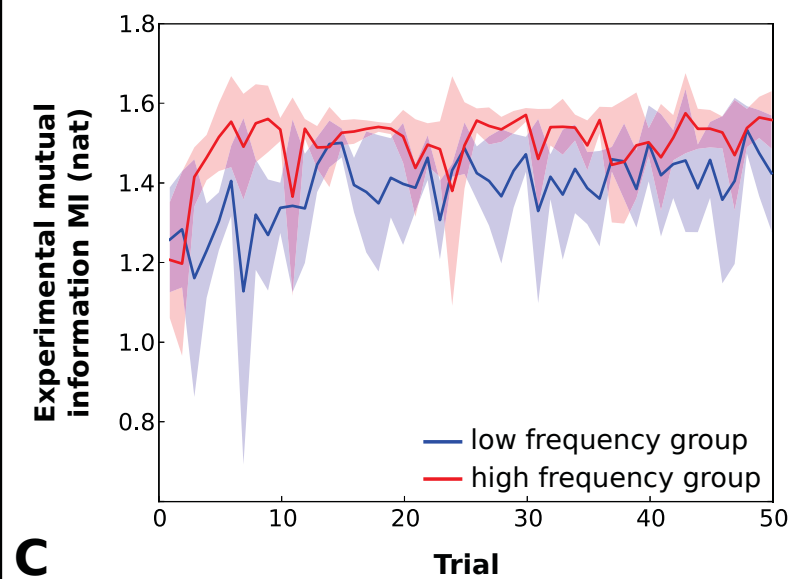
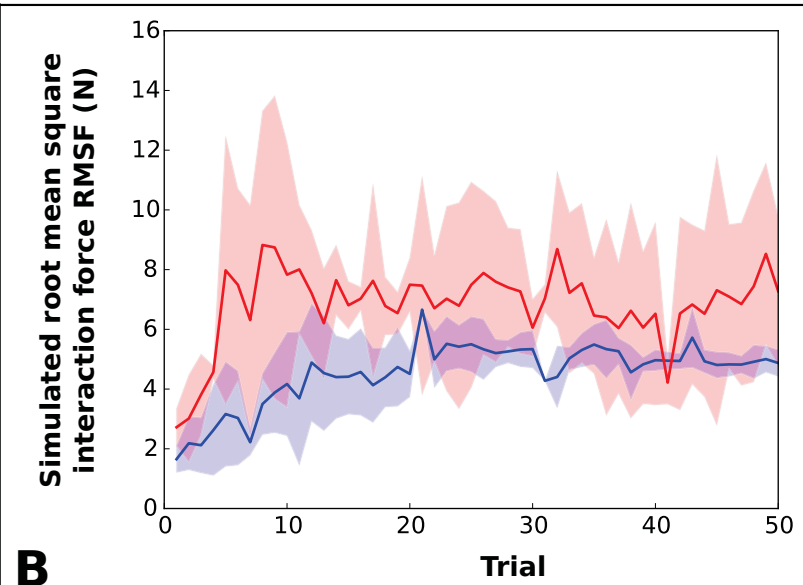
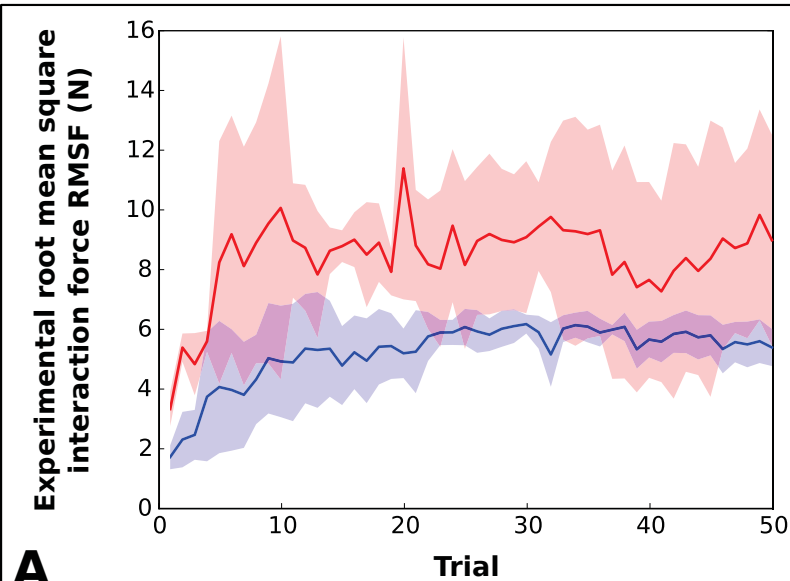


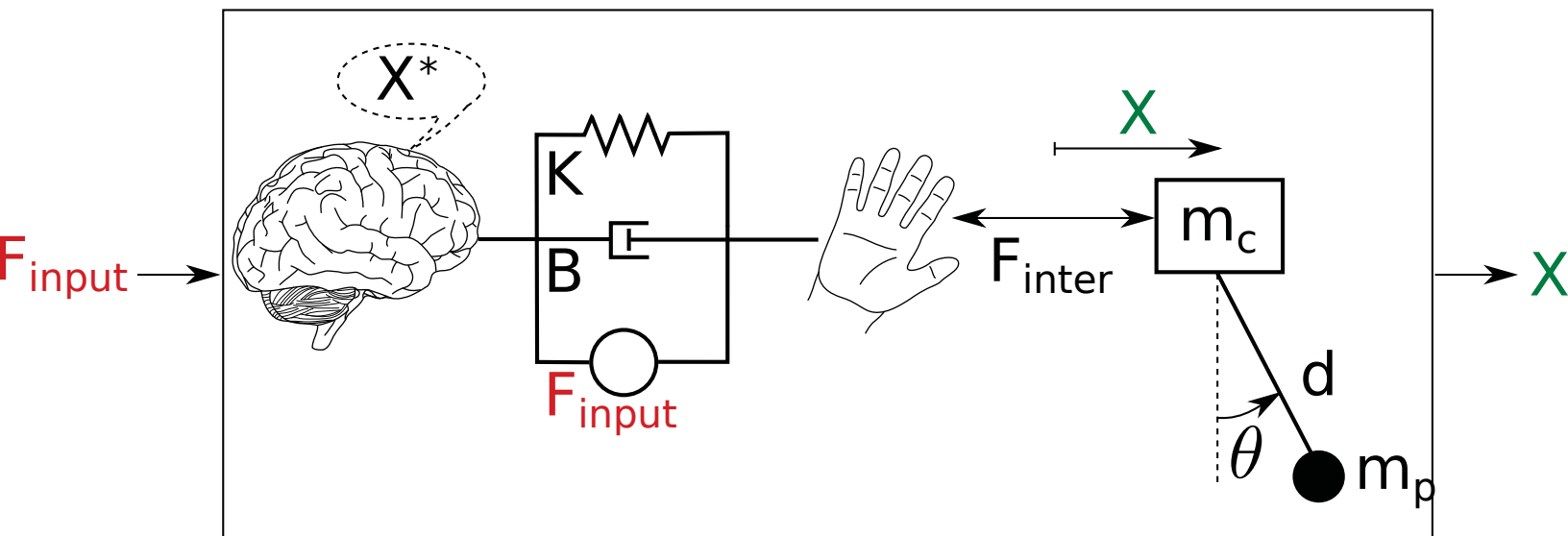


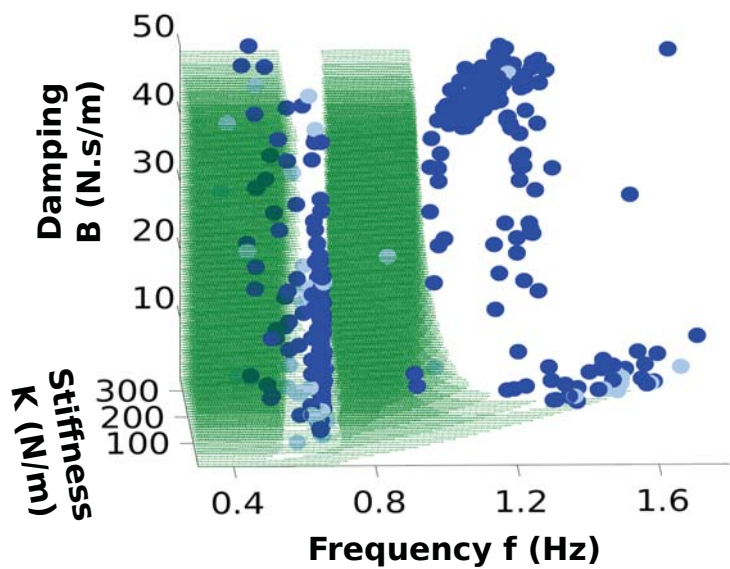


Experimental Results

Simulation Results



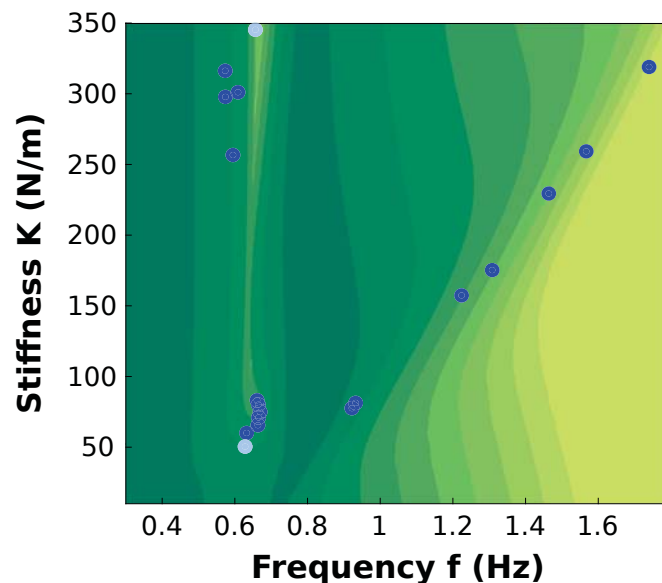




Interaction force

Simulated data
 ● $RMSF < 3$ N

Experimental data
 ● $C < 0.15$
 ● $0.15 < C < 0.20$

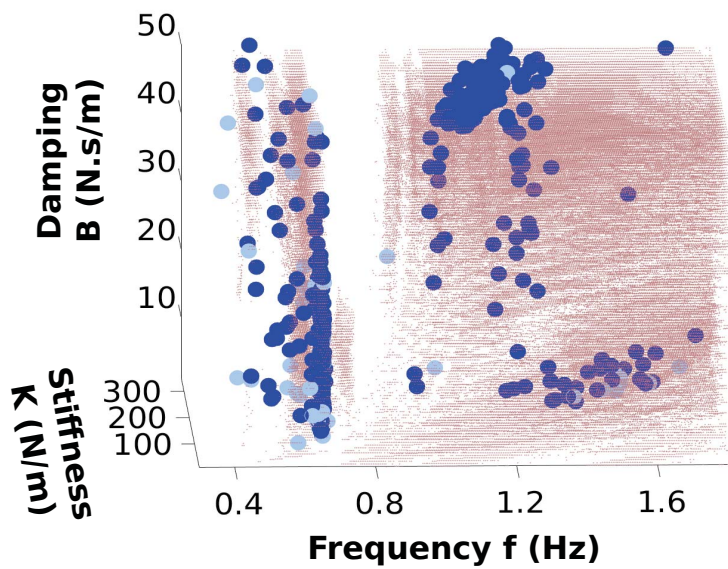


Root mean square force RMSF (N)
 2 4 6 8 10 12 14

● Experimental data point $C < 0.15$
 ● Experimental data point $0.15 < C < 0.20$

A

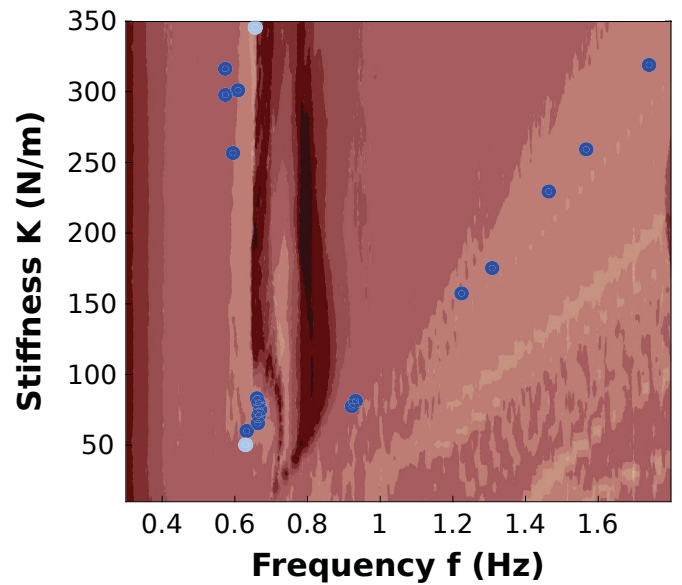
B



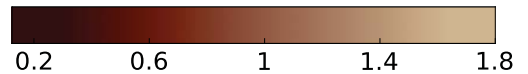
Mutual information

Simulated data
 ● $MI > 1.2$ nat

Experimental data
 ● $C < 0.15$
 ● $0.15 < C < 0.20$



Mutual information MI (nat)



● Experimental data point $C < 0.15$
 ● Experimental data point $0.15 < C < 0.20$

